Search for heavy Majorana neutrinos and right-handed W gauge bosons in 13 TeV proton-proton collisions at the LHC

Oda Kristin Berg Langrekken

Thesis submitted for the degree of
Master in Subatomic Physics
60 credits

Department of Physics
Faculty of mathematics and natural sciences

UNIVERSITY OF OSLO

Spring 2019

Search for heavy Majorana neutrinos and right-handed W gauge bosons in 13 TeV proton-proton collisions at the LHC

Oda Kristin Berg Langrekken

Search for heavy Majorana neutrinos and right-handed W gauge bosons in 13 TeV proton-proton collisions at the LHC

http://www.duo.uio.no/

Printed: Reprosentralen, University of Oslo

Abstract

The origin of the non-zero neutrino mass is an open question in the Standard Model (SM). A popular mechanism to explain the tininess of the neutrino mass is the Type-I Seesaw, where the lightness of the SM neutrinos is explained by the existence of heavy Majorana neutrinos. The Type-I Seesaw is naturally embedded in the Left-Right Symmetric Model (LRSM), which also introduces right-handed weak charged gauge bosons. In this thesis a search for heavy Majorana neutrinos in association with a $W_R^{\pm}$ boson is performed using data from pp collisions collected by the ATLAS detector at $\sqrt{s} = 13$ TeV. The search is performed in a final state with two same sign, same flavor leptons and two jets. No significant excess above the SM prediction is observed, and the exclusion limits are found to be consistent with the most recent search performed by the ATLAS collaboration. The excluded W_R masses extend to 4.2 TeV for N_R masses up to 2.1 TeV, while the highest excluded N_R mass is 2.7 TeV for $m_{W_R} = 3.6$ TeV.

Acknowledgements

First and foremost I would like to thank my supervisor Farid Ould-Saada for first introducing me to high energy particle physics when I was a bachelor student and constantly exposing me to new knowledge ever since - both through courses and during the work on my master thesis. I would also like to thank my co-supervisor Magnar Kopangen Bugge for great suggestions and ideas whenever I was stuck and for always keeping the threshold low for asking all types of questions.

I am also grateful to Eirik Gramstad, who provided me with the fakes estimation used in this thesis, and to Knut Oddvar Høie Vadla for always taking the time to answer my many, many questions.

Thank you to the rest of the HEPP group for countless quizzes, and thank to Mona and Helén for always being available for a hug.

Finally this year would have been a lot less productive without Johanne, who makes sure I get out of bed in the morning. I would also like to thank my parents for feeding me every Sunday.

Contents

Introduction

The neutrinos are elementary particles, and their properties and interactions are described by the Standard Model (SM) of particle physics. In the SM the neutrino is a massless particle. The discovery of neutrino oscillations have confirmed that at least two of the neutrinos do in fact have a non-zero, although very small, mass. The origin of the small neutrino mass is not currently understood. Certain theories beyond the SM (BSM) predict the existence of heavy right-handed Majorana neutrinos, and the small mass of the SM neutrinos are explained by the Seesaw Mechanism in these theories.

In this thesis a search for heavy Majorana neutrinos and and right-handed charged gauge bosons is performed within the theoretical framework of the Left-Right Symmetric Model (LRSM). The LRSM introduces new heavy gauge bosons Z' and $W_R^{\pm}$. In the process considered a heavy Majorana neutrino is produced in the decay of a $W_R^{\pm}$ boson, and subsequently decays to a lepton and virtual $W_R^{\pm}$ boson. The resulting final state consists of two same flavor leptons and two jets. Due to Majorana nature of the neutrino, the final state leptons have a 50% probability of having the same sign. This is a quite unique signature as lepton number is a conserved quantity in SM processes, and the search is performed solely in the same sign channel.

The search is performed using data from $\sqrt{s} = 13$ TeV proton-proton collisions at the LHC, collected by the ATLAS detector in 2015 and 2016, corresponding to an integrated luminosity of 36 fb^{-1}. Very little SM background is expected for the same sign channel, and the search is highly sensitive to the LRSM signal.

In the first part of the thesis some particle physics theory is presented. Neutrinos and neutrino oscillations are discussed in chapter 1, while a brief introduction to the Standard Model is given in chapter 2. Chapter 3 introduces the Majorana neutrino and its role in the LRSM.

The second part of the thesis considers the production and detection of Majorana neutrinos. The Keung-Senjanovic process is introduced in chapter 4. Chapter 5 is about the kinematics of particle collisions and important properties of the proton-proton collisions at the LHC. The interactions of particles with matter and how particles are reconstructed and identified using the ATLAS detector are discussed in chapter 6.

The analysis is presented in the third and last part of the thesis. The analysis procedure and the different sources of background are discussed in chapter 7, before the selection of signal events and the definition of the signal region are explained in chapter 8. The estimation of the background is performed in chapter 9, while the results of the search are finally presented in chapter 10.

Part I

The Neutrino in the Standard Model and Beyond

Chapter 1

The Neutrino

The three neutrinos ν_e, ν_μ and ν_τ are what we call elementary particles, which means that (at least as far as we know) they are ultimate constituents of the Universe and cannot be divided into smaller particles. Neutrinos carry spin-1/2 and are what we know as *fermions*, or *matter particles*. The neutrinos and their interactions are described by the Standard Model (SM), which classifies all the elementary particles and describes their interactions. Among the elementary particles the neutrinos are unique in many ways:

1. They are electrically neutral and do not carry color charge, which means that they only interact weakly. Although they are stable particles, the fact that they do not interact through the electromagnetic or the strong interaction means that they are the only stable matter particles that are not actually a constituent of matter. Neutrinos play an important role in processes where matter is transformed, such as fusion reactions in the Sun and nuclear β-decay.

2. Because the neutrinos do not carry electric charge it is the only fermion that could be a Majorana particle, a particle which is its own antiparticle.

3. Neutrinos have only been observed with left-handed chirality (and antineutrinos only with right-handed chirality), which is a consequence of the complete breaking of parity in the weak interaction. Since the mediators of the charged current, the $W^\pm$ bosons, only couple to left-handed fermions and right-handed antifermions, right-handed neutrinos do not participate in any of the Standard Model interactions. The right-handed neutrino was therefore not included when the Standard Model was formulated. As mass terms couple left- and right-handed states, the neutrinos are the only fermions that are considered massless by the SM.

The last item is particularly interesting as the discovery of neutrino oscillations have shown that neutrinos are in fact massive. When travelling over larger distances the neutrinos have a probability to change flavor, meaning that a neutrino produced as e.g. an electron neutrino, ν_e, can transform into a muon neutrino, ν_μ, or a tau neutrino, ν_τ. This implies that the neutrino flavor eigenstates differ from the neutrino mass eigenstates, and at least two of the neutrinos must have non-zero mass. Neutrino oscillations thus call for physics beyond the Standard Model.

1.1 Neutrino oscillations

The neutrinos come in three different flavors: the electron neutrino ν_e, the muon neutrino ν_μ and the tau neutrino ν_τ. They are named after the charged lepton to which they are associated, the electron e, the muon μ and the tau lepton τ (the charged leptons will be introduced in section 2.1). All leptons are assigned a lepton number L of +1, while antileptons are assigned a lepton number -1. In addition each flavor is assigned a lepton flavor number L_l (where $l = e, \mu$ or τ) of +1 while the antileptons carry a lepton flavor number of -1. In all Standard Model interactions, the lepton number is observed to be conserved both in total and for each lepton flavor separately. The muon neutrino is then defined as the neutrino produced alongside a muon in the decay of a $W^\pm$ boson, $W^+ \to \mu^+\nu_\mu$ or $W^- \to \mu^-\bar{\nu_\mu}$, thus ensuring conservation of the muon lepton number.

The 2015 Nobel Prize in physics recognized the discovery of neutrino oscillations by the Super-Kamiokande [1] and the SNO [2] experiments. The SNO experiment demonstrated that atmospheric neutrinos and the flux of neutrinos from β-decay in the Sun have large ν_μ and ν_τ components. Since only electron neutrinos are produced in the nuclear fusion processes in the Sun, the results from the experiments show that a neutrino produced with a specific lepton flavor can transform to a different flavor when traveling over large distances.

The neutrino flavor transformations can be explained by the quantum mechanical phenomenon of neutrino oscillations, which implies that the neutrino flavor states (ν_e, ν_μ and ν_τ) are linear combinations of the mass eigenstates (ν_1, ν_2 and ν_3). The flavor states can be related to the mass eigenstates by a unitary transformation

$$\begin{pmatrix} \nu_e \\ \nu_\mu \\ \nu_\tau \end{pmatrix} = \begin{pmatrix} U_{e1} & U_{e2} & U_{e3} \\ U_{\mu 1} & U_{\mu 2} & U_{\mu 3} \\ U_{\tau 1} & U_{\tau 2} & U_{\tau 3} \end{pmatrix} \begin{pmatrix} \nu_1 \\ \nu_2 \\ \nu_3 \end{pmatrix}$$

where the matrix U is the PMNS matrix. The PMNS matrix can be expressed in terms of three mixing angles θ_{12}, θ_{13} and θ_{23} [3]:

$$\begin{pmatrix} U_{e1} & U_{e2} & U_{e3} \\ U_{\mu 1} & U_{\mu 2} & U_{\mu 3} \\ U_{\tau 1} & U_{\tau 2} & U_{\tau 3} \end{pmatrix} = \begin{pmatrix} c_{12}c_{13} & s_{12}c_{13} & s_{13}e^{-i\delta} \\ -s_{12}c_{23} - c_{12}s_{23}s_{13}e^{i\delta} & c_{12}c_{23} - s_{12}s_{23}s_{13}e^{i\delta} & s_{23}c_{13} \\ s_{12}s_{23} - c_{12}c_{23}s_{13}e^{i\delta} & -c_{12}s_{23} - s_{12}c_{23}s_{13}e^{i\delta} & c_{23}c_{13} \end{pmatrix}$$

where $c_{ij} = \cos\theta_{ij}$, $s_{ij} = \sin\theta_{ij}$ and δ is the Dirac CP violation phase.

If the masses of the three mass eigenstates are not the same, the phases of the mass eigenstates propagate at different rates and neutrino oscillations occur. The discovery of neutrino oscillations thus confirm that the three neutrino mass states have different mass, which means at least two of the neutrinos must have non-zero masses.

Although the interpretation of neutrino oscillations is that the neutrinos must be massive, their masses are several orders of magnitude smaller than masses of the other known elementary particles. It is not currently understood why the neutrino mass is so small. Perhaps the most popular theory to explain the tininess of the neutrino mass is the Seesaw Mechanism, which will be the subject of section 3.1.3.

Chapter 2

The Standard Model

The Standard Model (SM) [4, 5, 6, 7, 8, 9] is a gauge theory based on the symmetry group $SU(3)_C \otimes SU(2)_L \otimes U(1)_Y$. It classifies all known elementary particles and describes the fundamental interactions between them, and has been incredibly successful in explaining experimental results, even predicting several particles before their discovery. The final particle predicted by the SM, the Higgs boson, was discovered by the ATLAS [10] and CMS [11] collaborations in 2012.

The SM describes three of the four fundamental interactions. The electromagnetic interaction is described by Quantum Electrodynamics (QED), the strong force by Quantum Chromodynamics (QCD) and the weak force by the Standard Electroweak theory, which is a unified description of the electromagnetic and weak interactions. The only fundamental force not included in the Standard Model is gravity, as a renormalizable quantum theory has not yet been formulated for gravity.

Although the SM has been very successful, the discovery of neutrino oscillations provides evidence for physics beyond the Standard Model (BSM). In this chapter a brief introduction to the Standard Model is given in an attempt to explain why the non-zero neutrino mass is an issue. First the elementary particles and their interactions are introduced. Then the gauge principle is briefly explained using the $U(1)$ symmetry of QED as an example. Finally I discuss the most relevant aspects of the Electroweak Unification and the Higgs mechanism.

2.1 The Elementary Particles and their Interactions

Neutrinos are of course not the only elementary particles. Nature is built up of atoms, which consist of a negatively charged electron orbiting a positively charged nucleus. The nucleus is made up of protons and neutrons, which are bound states of u and d quarks. Together with the electron neutrino, ν_e, the electron, the u quark and the d quark make up the first generation of elementary fermions, which are particles with half-integer spin known as matter particles.

The gauge bosons, knows as force particles, are elementary particles with integer spin. The gauge bosons are the mediators of the three fundamental interactions included in the Standard Model and carry spin-1. Among them we have the well-known photon γ, which

is the quantum of the electromagnetic radiation and the carrier of the electromagnetic interaction that binds the electron to the nucleus.

For each particle there exists a corresponding antiparticle which has the same mass and spin as the particle but opposite additive quantum numbers, most notably opposite electric charge. The antiparticle of the electron e^-, which has charge $-1e$, is the positron e^+ of charge $+1e$, where e is the elementary charge. Because of the difference in charge particle and antiparticle are distinguishable, i.e. different particles, for all charged fermions. Such particles are called Dirac particles, meaning that particle and antiparticle are distinct. Particles with no electric charge, such as the three neutrinos, have the potential of being their own anti-particle, a so-called Majorana particle.

2.1.1 Bosons

The elementary particles interact with each other through four fundamental interactions: the weak and strong interactions, the electromagnetic interaction and the gravitational interaction. In the Standard Model three of these interactions are understood as the exchange of gauge bosons, particles which carry spin-1 (the proposed mediator of the gravitational interaction - the graviton - has spin-2, but this particle is yet unconfirmed). The gauge bosons of a certain interaction couple to particles that carry the charge of the interaction, which corresponds to the conserved quantity under transformations of the underlying gauge group.

The photon

The mediator of the electromagnetic interaction, which is responsible for the attraction between negatively and positively charged particles that makes the electron orbit the nucleus, is the massless photon. The photon couples to all particles that carry electric charge. As the photon itself is electrically neutral, it does not couple to itself.

The gauge group of the electromagnetic interaction is $U(1)$ and the conserved quantity associated with symmetry under $U(1)$ transformations is the electric charge, which is thus conserved in all particle interactions.

The gluons

The strong interaction, which keeps quarks confined in hadrons and binds the neutrons and protons in the nucleus together, is mediated by eight gluons that couple to all particles carrying color charge. The gauge group of the strong interaction is $SU(3)_C$. Color charge is conserved in all particle interactions.

Like the photon the gluons have no mass and are electrically neutral. They do however carry color charge, which means that gluons can couple to each other.

The weak gauge bosons

The weak interaction is mediated by the $W^{\pm}$ and Z bosons. Unlike the photon and the gluons the gauge bosons of the weak interaction are massive, with $m_W \approx 80$ GeV and $m_Z \approx 91$ GeV[3]. The $W^{\pm}$ bosons also carry electric charge $\pm 1e$, while the Z boson is neutral. The weak gauge bosons couple to all fermions.

The weak interaction is quite special in that it is the only interaction that violates conservation of parity (left-right symmetry) and charge conjugation (particle-antiparticle symmetry), as the charged weak gauge bosons couple exclusively to left-handed fermions and right-handed antifermions. The charged current of the weak interaction, mediated by the $W^{\pm}$ bosons, is also the only interaction where quark flavor number is not conserved.

The Higgs boson

The final fundamental boson is the Higgs boson, which is a scalar boson with spin-0 and mass $m_H \approx 125$ GeV [3]. It is connected to the Brout-Englert-Higgs mechanism through which the electroweak symmetry is spontaneously broken and the weak gauge bosons, quarks and charged leptons acquire mass.

2.1.2 Fermions

The remaining elementary particles are the fermions, which carry spin 1/2 and are known as matter particles. The fermions can further be divided into groups according to what charges they carry, which determines how they interact.

Quarks

The quarks carry color charge, weak isospin and electric charge, and hence interact via the strong, weak and electromagnetic interactions. We have already mentioned the up-quark (u) and the down-quark (d), which are the elementary constituents of the protons and the neutrons of the atomic nucleus. The up-quark carries electric charge $+2/3e$, while the down-quark carries electric charge $-1/3e$, thus giving the proton (uud) and electric charge of $+1e$ and making the neutron (udd) electrically neutral.

All in all we have six flavors of quarks: up u, down d, charm c, strange s, top t and bottom b. The charm and top quarks can be seen as heavier "twins" of the up quark, as they carry the same quantum numbers (except for the quark flavor number) but have higher mass, with $m_t > m_c > m_u$. Analogously the strange and bottom quarks are heavier twins of the down quark, with $m_b > m_s > m_d$. The quarks can be grouped into three generations,

$$\begin{matrix} 1^{\text{st}} & 2^{\text{nd}} & 3^{\text{rd}} \\ \begin{pmatrix} u \\ d \end{pmatrix} & \begin{pmatrix} c \\ s \end{pmatrix} & \begin{pmatrix} t \\ b \end{pmatrix} \end{matrix}$$

For each quark, q, there exists an antiquark, $\bar{q}$, which has the same mass and spin but opposite additive quantum numbers.

In addition to electric charge the quarks carry weak isospin, making them interact through the weak interaction. Due to their larger mass all quarks but the up-quark are not stable, but will decay to fermions of the first family through the absorption or emission of W bosons.

Lastly the quarks are the only fermions that have color, the charge of the strong interaction. A quark can have one of three different colors (red, green or blue), while an antiquark has anticolor (antired, antigreen or antiblue). Only colorless states exist in Nature. Quarks can thus not be observed as free particles, but hadronize to form colorless states, so-called hadrons. The only exception is the top quark, which is so massive ($m_T \approx 173$ GeV [3]) that it decays before hadronizing. Colorless states are achieved by combining three quarks, (qqq), or by combining a quark with an antiquark, $(q\bar{q})$. Three quark states are known as baryons and include particles such as the proton and the neutron, while quark-antiquark states are called mesons. Each baryon is assigned a baryon number B of $+1$ while the antibaryons have $B = -1$ and the mesons have $B = 0$. The baryon number is conserved in all known interactions.

Leptons

The fermions that do not carry color charge are known as leptons. The leptons come in three different flavors: the electron e^-, the muon, μ^-, the tau lepton, τ^- which all carry an electric charge of $-1e$, while their antiparticles (denoted as e^+, μ^+ and τ^+) have electric charge $+1e$. For each of the three charged lepton there is a corresponding neutrino which is electrically neutral. All leptons are assigned a lepton number, L, of $+1$, while the antileptons have lepton number -1. The lepton number is conserved in all of the known particle interactions.

As for the quarks, the leptons can be grouped into three generations

$$\begin{matrix} 1^{\text{st}} & 2^{\text{nd}} & 3^{\text{rd}} \\ \begin{pmatrix} e^- \\ \nu_e \end{pmatrix} & \begin{pmatrix} \mu^- \\ \nu_\mu \end{pmatrix} & \begin{pmatrix} \tau^- \\ \nu_\tau \end{pmatrix} \end{matrix}$$

The charged leptons mostly share the same quantum numbers, but differ in lepton flavor number and mass. For the charged fermions the masses increase with generation number, with $m_\tau > m_\mu > m_e$. The different neutrino flavors do also differ in mass, but the mass hierarchy is not known.

All leptons carry weak isopsin, and thus interact weakly. Muons and tau leptons are consequently not stable as they will decay through the weak interaction.

The elementary particles and their interactions are summarized in figure 2.1.

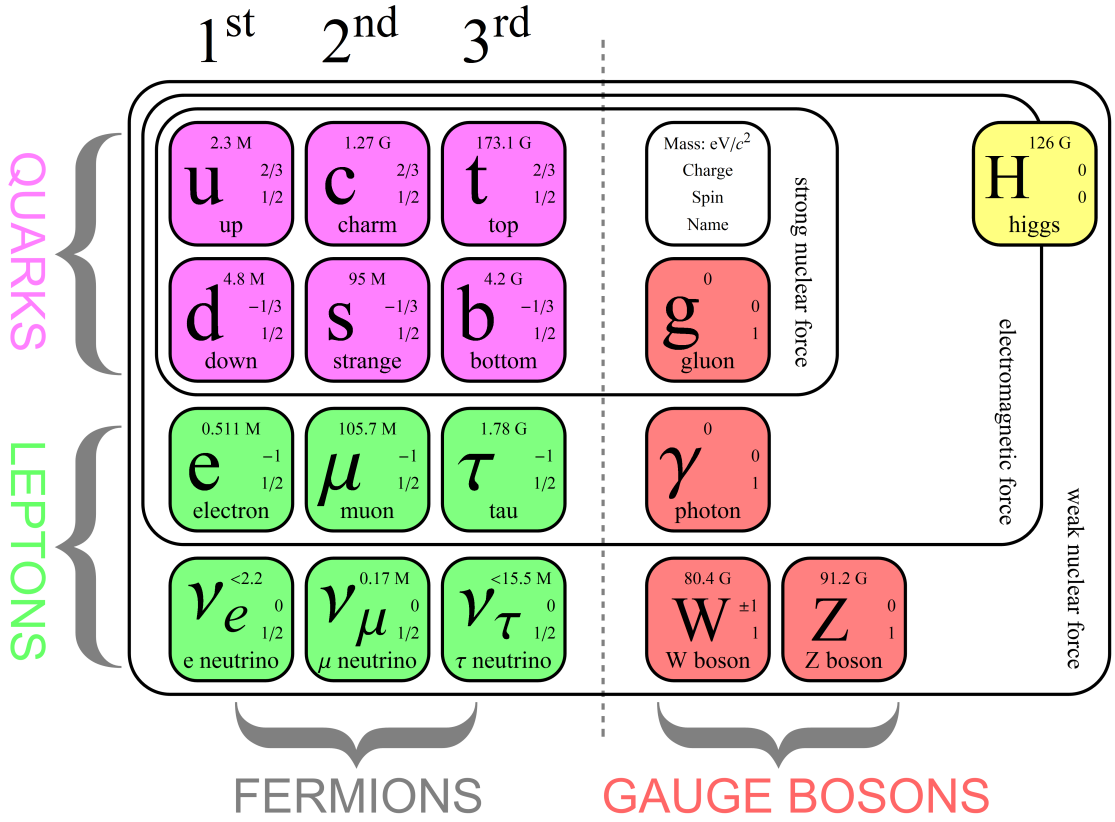

Figure 2.1: The particle content of the Standard Model, taken from [12].

2.2 The gauge principle and QED

The Standard Model is a quantum field theory [13], combining special relativity and quantum mechanics. In quantum field theory particles are described as discrete excitations of a quantum field, with the field as the fundamental component. Each of the elementary particles is associated with its own field, so we have a quark field, a Z-boson field, a neutrino field etc. The dynamics of these fields are expressed in terms of the Lagrangian density (from here on simply called the Lagrangian), $\mathcal{L}$. The Lagrangian of a free Dirac field ψ, which describes fermions, is

$$\mathcal{L}_0 = \bar{\psi}(i\gamma^\mu \partial_\mu - m)\psi = i\bar{\psi}\gamma^\mu \partial_\mu \psi - m\bar{\psi}\psi \tag{2.1}$$

where the first term corresponds to the kinetic energy of the field, while the second term is the self-energy, or mass term.

The previously mentioned gauge groups and the conserved currents of their associated interactions are related to symmetries of the Lagrangian. As an example the Lagrangian $\mathcal{L}_0$ above is invariant under global $U(1)$ transformations,

$$\psi(x) \to e^{i\alpha}\psi(x) \tag{2.2}$$

where α is a real constant.

The Lagrangian is however not invariant under local $U(1)$ transformations

$$\psi(x) \to e^{i\alpha(x)}\psi(x) \tag{2.3}$$

because

$$\partial_\mu \psi(x) = e^{i\alpha(x)}[\partial_\mu + i\partial_\mu \alpha(x)]\psi(x) \tag{2.4}$$

To ensure invariance of the Lagrangian under local $U(1)$ transformations, one adds a spin-1 field $A_\mu(x)$ transforming as

$$A_\mu(x) \to A_\mu(x) - \frac{1}{e}\partial_\mu \alpha(x) \tag{2.5}$$

and defines the covariant derivative

$$D_\mu \equiv \partial_\mu + ieA_\mu(x) \tag{2.6}$$

where e, the elementary charge, has been extracted from the constant α.

For the vector field A_μ to be a true propagating field one needs to add a kinetic term that keeps the Lagrangian invariant. We define the kinetic term as

$$\mathcal{L}_{kin} = -\frac{1}{4}F_{\mu\nu}F^{\mu\nu} \tag{2.7}$$

where $F_{\mu\nu}$ is the electromagnetic field strength, $F_{\mu\nu} = \partial_\mu A_\nu - \partial_\nu A_\mu$.

A mass term for the vector field is not allowed as it would violate the local $U(1)$ invariance.

Now, after demanding invariance under local $U(1)$ transformation, our we obtain the full Lagrangian

$$\mathcal{L} = \bar{\psi}(i\gamma^\mu D_\mu - m)\psi - \frac{1}{4}(F_{\mu\nu})^2 = \mathcal{L}_0 - \frac{1}{4}(F_{\mu\nu})^2 - e\bar{\psi}\gamma^\mu \psi A_\mu \tag{2.8}$$

which is the Lagrangian of Quantum Electrodynamics (QED).

The Lagrangian has been made invariant under local $U(1)$ transformations by adding a vector field and replacing the derivative with the covariant derivative. This introduces an interaction term (the last term in equation (2.8)) to the Lagrangian. The vector field is associated with the massless photon, while the interaction term corresponds to the well-known interaction vertex of QED:

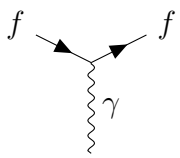

Figure 2.2: The basic vertex of QED, which couples a photon γ to charged fermions f. Both electric charge, lepton flavor number and quark flavor number are conserved at this vertex, so the incoming fermion carries the same lepton/quark flavor as the outgoing fermion. In this and all coming Feynman diagrams time is from left to right.

Demanding local gauge invariance necessitates introducing vector fields to the Lagrangian, with the vector fields being associated with the spin-1 gauge bosons. This is known as the gauge principle; localizing the global symmetry of the free Lagrangian leads to additional fields and additional terms which describes the interactions of the theory.

2.2.1 QCD

In the case of Quantum Chromodynamics (QCD) [14] eight gluons arise as excitations of the vector fields added to ensure invariance under local $SU(3)_C$ transformations. Additionally one gets interaction terms describing the coupling of the gluon to fermions carrying color charge and (as the $SU(3)_C$ group is non-abelian and the generators of the group do not commute) gluon self-interaction terms, shown in fig. 2.3.

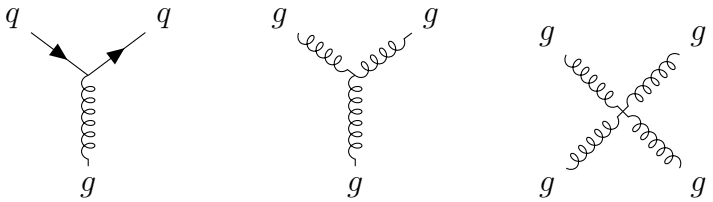

Figure 2.3: The primary vertices of QCD, showing from left to right a gluon coupling to quarks, a three-gluon vertex and a four-gluon vertex. Color charge, electric charge and quark flavor number are conserved at QCD vertices, so the incoming and outgoing quarks have the same quark flavor.

A mass term is forbidden by the gauge symmetry, and the gluons are predicted to be massless.

2.2.2 The Electroweak Interaction

The weak interaction is most easily explained through the electroweak theory [15], which is a unification of the electromagnetic and the weak interaction based on the symmetry group $SU(2)_L \times U(1)_Y$, where L refers to left-handed fields and Y is the weak hypercharge

$$Y = 2(Q + I_3) \tag{2.9}$$

where Q is the electric charge and I_3 is the third component of the weak isopsin.

Gauge invariance of the free Lagrangian under local transformations under the electroweak gauge group introduces four new gauge fields to the theory. Linear combinations of these gauge fields correspond to the photon and the $W^{\pm}$ and Z bosons of the weak interaction. The gauge bosons couple to the fermions through the vertices shown in fig. 2.4

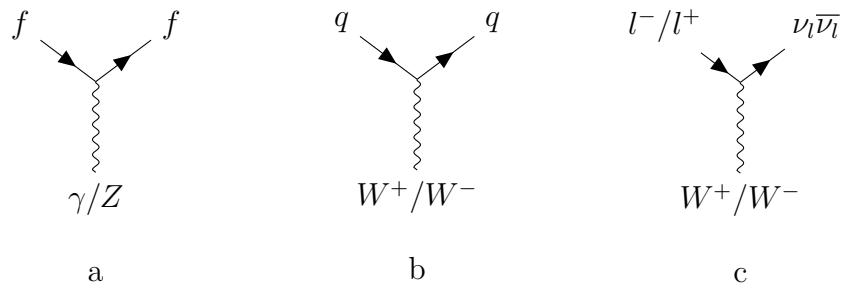

Figure 2.4: The primary vertices of the electroweak interaction that includes fermions. Diagram a shows fermions coupling to the neutral bosons of the electroweak theory, the photon γ and the Z boson. The photon couples only to charged particles, while the Z boson also couples to neutrinos. Diagram b and c show the coupling of the charged bosons $W^{\pm}$ to fermions. Charge is conserved in all electroweak interactions, so the incoming and outgoing quarks in diagrams b and c differ by one unit of electric charge. The charged currents of the weak interaction are thus the only interaction where quark flavor is not conserved. Lepton flavor is however conserved, so the charged lepton and the neutrino in diagram c have the same lepton flavor.

In addition the non-commutivity of the generators of the electroweak gauge group leads to gauge boson self-interactions, shown in fig. 2.5.

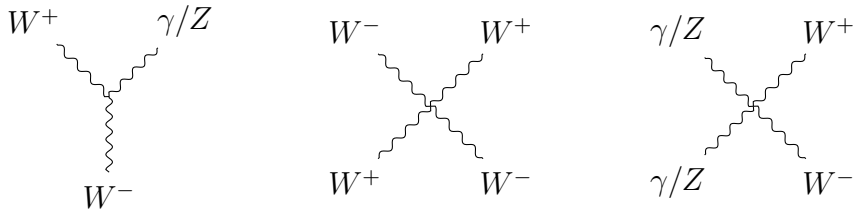

Figure 2.5: The primary gauge boson self-interaction vertices of the electroweak theory.

When the electroweak theory was formulated, it was already known from experiments that the charged weak gauge bosons couple exclusively to left-handed fermions and right-handed antifermions. Hence one distinguishes between left- and right-handed fields when constructing the charged current Lagrangian of the electroweak theory, and the left-handed components of the spinors are grouped in isospin doublets while the right-handed component is an isopsin singlet. For the first fermion family, the doublets and singlets are:

$$Q_L = \begin{pmatrix} u \\ d \end{pmatrix}_L, \qquad l_L = \begin{pmatrix} \nu \\ e \end{pmatrix}_L, \qquad e_R, \qquad u_R, \qquad d_R \tag{2.10}$$

Notice that there is no right-handed neutrino field. Because the right-handed neutrino carries no isospin or electric charge, it was simply left out of the theory.

Once again a mass term for the gauge bosons is forbidden by the electroweak gauge symmetry. This is problematic as the $W^{\pm}$ and Z bosons are massive. In addition the fermion mass terms breaks the gauge symmetry as they couple left- and right-handed fields.

To generate masses for the gauge bosons a complex scalar field ϕ that transforms as an $SU(2)_L$ doublet is added to the Lagrangian.

$$\phi \equiv \begin{pmatrix} \phi^+ \\ \phi^0 \end{pmatrix} \tag{2.11}$$

The vacuum expectation value of the neutral component is chosen to be non-zero

$$\langle \phi^+ \rangle = 0, \qquad \langle \phi^0 \rangle = \frac{v+h}{\sqrt{2}} \tag{2.12}$$

where v is a constant and h is the Higgs field, which is associated with the Higgs boson.

When the scalar field develops a non-zero vacuum expectation value, the $SU(2)_L \otimes U(1)_Y$ symmetry is spontaneously broken down to the symmetry group of QED

$$SU(2)_L \otimes U(1)_Y \rightarrow U(1)_{QED} \tag{2.13}$$

and the $W^\pm$ and Z bosons acquire mass, while the photon remains massless. This is known as the Brout-Englert-Higgs mechanism [8, 9].

The masses of the gauge bosons are proportional to the vacuum expectation value of the Higgs field, with

$$m_W = \frac{1}{2} v g_W \qquad m_Z = \frac{1}{2} v \sqrt{g_W^2 + g_e^2} \tag{2.14}$$

where g_e and g_W are the coupling strengths of the electromagnetic and weak interaction respectively.

The fermions also acquire mass by their Yukawa couplings to the Higgs doublet ϕ:

$$\mathcal{L}_Y = h_u \overline{Q}_L \tilde{\phi} u_R + h_d \overline{Q}_L \phi d_R + h_e \bar{l}_L \phi e_R + h.c. \tag{2.15}$$

where h_f is the Yukawa coupling of the fermion and $\tilde{\phi}$ is the complex conjugate of ϕ.

When the electroweak symmetry is broken down due to the vacuum expectation of the Higgs doublet ϕ, $\langle \phi \rangle = v$, the Yukawa Lagrangian reduces to mass terms for the fermions. Taking the electron as an example, we get the term

$$\mathcal{L}_Y^e = m_l \bar{e} e \tag{2.16}$$

where m_e is the mass of the electron

$$m_e \equiv \frac{h_e v}{\sqrt{2}} \tag{2.17}$$

The lepton mass is thus determined by its Yukawa coupling, and differences in Yukawa couplings leads to different masses across lepton families.

Finally the reader should notice that the absence of a right-handed neutrino field leads to a massless neutrino.

Chapter 3

Beyond the Standard Model

3.1 The neutrino mass

A neutrino mass term is not explicitly forbidden in the Standard Model the way mass terms for the photon and the gluons are forbidden by the requirement of gauge invariance. The right-handed neutrino was simply left out by choice as it does not participate in any of the fundamental interactions, and the absence of the right-handed field was not regarded as a problem when the Standard Model was formulated because the neutrinos were considered massless. Now that we know that the neutrinos are massive, a mass term must be added to the SM Lagrangian.

3.1.1 The neutrino as a Dirac particle

For a Dirac particle, for which particle and antiparticle are distinct, the associated field is described by a four-component Dirac spinor ψ. The Dirac field can be expressed in terms of a a left- and a right-handed part

$$\psi = \begin{pmatrix} \psi_L \\ \psi_R \end{pmatrix} \tag{3.1}$$

where ψ_L and ψ_R are two-component Weyl spinors.

In the Standard Model the neutrino field has no right-handed part and it is represented by a left-handed Weyl field. As the Dirac mass term mixes the left- and right-handed fields, the SM does not include a Dirac mass term for the neutrinos.

Assuming the neutrino is a Dirac particle a Dirac mass term can be generated for the neutrinos by simply adding right-handed neutrinos ν_R to the theory:

$$\mathcal{L} = -m_\nu(\overline{\nu}_R\nu_L + \overline{\nu}_L\nu_R) \tag{3.2}$$

After electroweak spontaneous symmetry breaking the neutrinos get a mass

$$m_\nu = \frac{h_\nu v}{\sqrt{2}} \tag{3.3}$$

So once again the mass of the neutrino is completely determined by its Yukawa coupling constant, h_ν. The neutrino mass is known to be very small, several orders of magnitude smaller than the masses of the charged leptons, which requires extremely small Yukawa couplings, $h_\nu \leq 10^{-12}$ for neutrino masses less than 1 eV [16]. There is no apparent reason why the Yukawa couplings of the neutrinos should be so much smaller than the couplings of the charged leptons, which indicated that there might be another mechanism that generates the neutrino mass.

With no further extensions to the Standard Model a Dirac right-handed neutrino would be sterile, i.e. coupling exclusively to the Higgs boson, which makes them highly difficult to detect.

3.1.2 The neutrino as a Majorana particle

As the neutrinos are electrically neutral they could be their own antiparticles, so-called Majorana fermions. A left-handed antifermion is the CP conjugate of the right-handed fermion [17]

$$\psi_L^c = C\overline{\psi}_R^T \tag{3.4}$$

where C is the charge conjugation matrix. For a Majorana fermion $\psi^c = \psi$ and, assuming the neutrino is a Majorana fermion, the neutrino field can be expressed solely in terms of either left- or right-handed fields through a Majorana spinor [18]

$$\psi_\nu = \begin{pmatrix} \overline{\nu_R^c} \\ \nu_R \end{pmatrix} \tag{3.5}$$

where $\overline{v_R^c}$ is the CP conjugate of the right-handed neutrino, corresponding to a left-handed anti-neutrino. For a Majorana fermion any term coupling the components of the Majorana spinor will be Lorentz invariant, so a Majorana mass term can be added

$$\mathcal{L}_M = -\frac{1}{2} M(\overline{\nu_R^c}\nu_R + \overline{\nu_R}\nu_R^c) \tag{3.6}$$

where M is the Majorana mass. Because the right-handed neutrinos are singlets under the SM gauge group, the Majorana mass term is automatically gauge invariant and the masses M are not constrained by gauge symmetry and can be arbitrarily large.

If the neutrino is a Majorana fermion, the global $B - L$ (baryon number minus lepton number) symmetry of the Standard Model would be broken. There is no evident reason why baryon and lepton number are conserved, and the asymmetry between matter and antimatter in the Universe actually hints at baryon number non-conserving processes.

3.1.3 The Type-I Seesaw Mechanism

In the type I seesaw mechanism [19] the neutrinos are Majorana fermions. Three right-handed neutrinos, ν_R, one for each left-handed neutrino, ν_L, are added to the theory. After electroweak symmetry breaking, one gets the following Yukawa for the neutrinos

$$\mathcal{L} = -\frac{1}{2}\left(M\overline{\nu_R^c}\nu_R + m_D\overline{\nu_L}\nu_R + m_D\overline{\nu_R^c}\nu_L^c\right) + h.c. \tag{3.7}$$

where $m_D = h_\nu v$ is the Dirac mass, assumed to be of the order of the charged lepton mass, and M is the Majorana mass. The properties of Majorana particles have been used to rewrite the Dirac mass term

$$\mathcal{L}_D = -m_\nu \overline{\nu_L} N_R + h.c. = -\frac{m_\nu}{2}(\overline{\nu_L} N_R + \overline{N_R^c}\nu_L^c) + h.c.$$

Equation 3.7 can be written more compactly in matrix form

$$\mathcal{L} = -\frac{1}{2}\begin{pmatrix}\overline{\nu_L} & \overline{\nu_R^c}\end{pmatrix}\begin{pmatrix}0 & m_D \\ m_D & M\end{pmatrix}\begin{pmatrix}\nu_L^c \\ \nu_R\end{pmatrix} + h.c. \tag{3.8}$$

The neutrino masses can be related through a mass matrix [16]

$$\mathcal{M} = \begin{pmatrix}0 & m_D \\ m_D & M_N\end{pmatrix} \tag{3.9}$$

Assuming $M_N \gg m_D$, the masses of the left- and right-handed neutrinos are

$$m_N \simeq M_N, \qquad m_\nu \simeq \frac{m_D^2}{M_N} \tag{3.10}$$

so the lightness of the left-handed neutrinos is explained by the existence of much heavier right-handed neutrinos.

3.2 The Left-Right Symmetric Model

Right-handed neutrinos and a type-I seesaw mechanism occur naturally in the Left-Right Symmetric Model (LRSM), which was first formulated by Mohapatra, Pati, Senjanović and Salam [20, 21, 22, 23]. The LRSM is a theory Beyond the Standard Model that attempts to restore parity symmetry at high energies by adding a right-handed equivalent to $SU(2)_L$. The full electroweak gauge group is then [24]

$$SU(2)_R \otimes SU(2)_L \otimes U(1)_{B-L},$$

where the SM formula for the electromagnetic charge

$$Q_{em} = I_3 + \frac{Y}{2} \tag{3.11}$$

has been replaced by

$$Q_{em} = I_{3L} + I_{3R} + \frac{B-L}{2} \tag{3.12}$$

which trades the hypercharge Y of the SM with the difference in baryon and lepton number, $B - L$.

In the LRSM both left- and right-handed fermion fields are grouped into doublets

$$Q_{L,R} = \begin{pmatrix}u \\ d\end{pmatrix}_{L,R}, \qquad l_{L,R} = \begin{pmatrix}\nu \\ e\end{pmatrix}_{L,R} \tag{3.13}$$

making them left-right symmetric.

Just as the $SU(2)_L$ group is associated with the weak gauge bosons $W_L^{\pm}$ and Z^0 coupling to left-handed fermions, the $SU(2)_R$ group is associated with new weak gauge bosons $W_R^{\pm}$ and Z' coupling to right-handed fermions, among them the so far unobserved right-handed neutrino, N.

To generate masses for the charged fermions the Higgs sector is extended with respect to the SM, and consists of a bi-doublet Φ and $SU(2)_{L,R}$ triplets $\Delta_{L,R}$

$$\Phi = \begin{pmatrix} \phi_1^0 & \phi_2^+ \\ \phi_1^- & -\phi_2^{0*} \end{pmatrix}, \qquad \Delta_{L,R} = \begin{pmatrix} \Delta^+/\sqrt{2} & \Delta^{++} \\ \Delta^0 & -\Delta^+/\sqrt{2} \end{pmatrix}_{L,R} \tag{3.14}$$

As parity is violated in the weak interaction, the left-right symmetry must be broken. The symmetry breakdown takes place in two steps. In the first step the symmetry is broken down to the electroweak gauge group of the Standard Model as the triplet $\Delta_{L,R}$ acquires a non-zero vacuum expectation value

$$\langle \Delta_L^0 \rangle = 0, \qquad \langle \Delta_R^0 \rangle = v_R \tag{3.15}$$

breaking the left-right symmetry down to the SM symmetry

$$SU(2)_R \times SU(2)_L \times U(1)_{B-L} \to SU(2)_L \times U(1)_Y \tag{3.16}$$

which generates masses for the W_R and the Z' bosons, and the right-handed neutrino N.

Then the electroweak group is broken down as the bi-doublet Φ develops a vacuum expectation value

$$\langle \Phi \rangle = \begin{pmatrix} \kappa_1 & 0 \\ 0 & \kappa_2 \end{pmatrix} \tag{3.17}$$

The electroweak gauge group is broken down to the $U(1)$ group of QED

$$SU(2)_L \times U(1)_Y \to U(1)_{QED} \tag{3.18}$$

and the $W_L^{\pm}$ and Z^0 bosons acquire mass.

The parity violation of the weak interaction (and the fact that the right-handed gauge bosons have not been observed) can be explained if the right-handed gauge bosons are much heavier that their left-handed counterparts, $m_{W_R} \gg m_{W_L}$, which translates to a difference in the vacuum expectation values. In other words:

$$m_{W_R} \simeq v_R \gg m_{W_L} \simeq v \tag{3.19}$$

where $v = \kappa_1^2 + \kappa_2^2$.

The coupling of the fermions to the W_R is then largely suppressed ($\sim m_{W_L}^2/m_{W_R}^2$ [25]), and the right-handed fermions behave as singlets. Parity becomes maximally violated as $m_{W_R} \to \infty$, making the left-right symmetric group indistinguishable from $SU(2)_L \times U(1)$ at low energies, in perfect accord with our observations of weak interaction processes.

3.2.1 Neutrinos in the LRSM

In versions of the LRSM which includes a Type-I Seesaw Mechanism [26], the neutrinos ν and N are Majorana fermions. The left- and right-handed lepton doublets are

$$l_L = \begin{pmatrix} \nu_L \\ e_L \end{pmatrix}, \qquad l_R = \begin{pmatrix} N_R \\ e_R \end{pmatrix} \tag{3.20}$$

The right-handed fields acquire mass after breaking of the left-right symmetry by their Yukawa coupling to the triplets Δ_R, corresponding to a Majorana mass term

$$\mathcal{L}_M = -h_\Delta v_R(\overline{N_R^c}N_R + \overline{N_R}N_R^c) \tag{3.21}$$

where h_Δ is the Yukawa coupling to the Δ_R.

A Dirac mass term is constructed as usual by the Yukawa coupling to the Higgs bi-doublet Φ, giving the neutrino mass term

$$\mathcal{L} = -\frac{1}{2}\left(h_\Delta v_R \overline{N_R^c}N_R + m_D\overline{\nu_L}N_R + m_D\overline{N_R^c}\nu_L^c\right) + h.c. \tag{3.22}$$

$$= -\frac{1}{2}\begin{pmatrix} \overline{\nu_L} & \overline{N_R^c} \end{pmatrix}\begin{pmatrix} 0 & m_D \\ m_D & h_\Delta v_R \end{pmatrix}\begin{pmatrix} \nu_L^c \\ N_R \end{pmatrix} + h.c. \tag{3.23}$$

which corresponds to a type-I seesaw with a Majorana mass $h_\Delta v_R$.

Using $h_\Delta v_R \simeq m_{W_R}$, the masses of the left- and right-handed neutrinos are related to the W_R mass by [26]

$$m_{\nu_l} \simeq \frac{m_l^2}{m_{W_R}}, \qquad m_N \simeq m_{W_R} \tag{3.24}$$

where $l = e, \mu, \tau$.

So the tininess of the mass of the left-handed neutrinos is related to the violation of parity in the weak interaction, as the left-handed neutrino mass tends to zero and parity is maximally violated when the mass of the W_R boson approaches infinity. In the LRSM both the neutrino mass and the parity violation of the weak interaction has a natural origin in the breaking of the left-right symmetry and the consequent mass difference of the right- and left-handed charged vector bosons.

Part II

Production and detection of Majorana neutrinos

Chapter 4

The Keung-Senjanović process

The process considered in this thesis is the Keung-Senjanović process (KS) (figure 4.1), first proposed by Wai-Kee Keung and Goran Senjanović [27] as a high-energy lepton number violating process to directly test the Majorana nature of the neutrino and confirm the existence of the left-right symmetry through the discovery of a W_R boson.

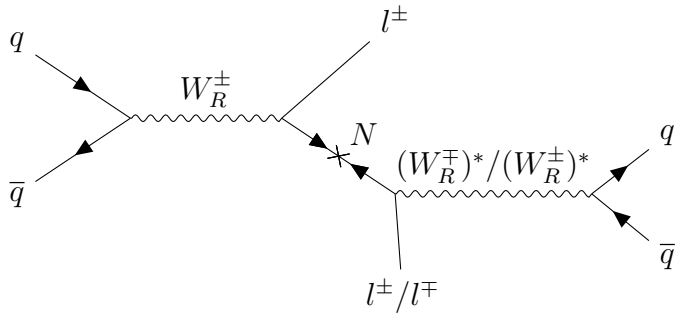

Figure 4.1: The Keung-Senjanović process where a heavy Majorana neutrino N is produced through the decay of a W_R boson. Because of the Majorana nature of the neutrino N, this process results in same sign and opposite sign leptons with equal probability.

In the Keung-Senjanović process a heavy Majorana neutrino is produced through the decay of a W_R boson, as illustrated in figure 4.1. In this thesis it is assumed that $m_{W_R} > m_{N_R}$, so the decay proceeds as follows

$$W_R \to lN \to llW_R^* \to llqq$$

where l is a charged lepton ($l = e, \mu, \tau$).

The decay products of the W_R boson and Majorana neutrino are two charged leptons and a quark-antiquark pair. The detectable products of a particle decay is known as its final state. As a quark cannot be observed as a free particle due to its color confinement, it hadronises after production and forms a bunch of particles travelling together. This particle bunch is known as a jet. So the final state of the Keung-Senjanović process is two leptons and two jets. In the case when $m_{W_R} \gg m_N$ the neutrino is boosted and the decay products of the neutrino can be reconstructed as one fat jet. The boosted topology is studied in separate analyses [28], and only the two lepton and two jets final state is

considered in this analysis. It will later be seen that this makes the search insensitive to small Majorana neutrino masses.

No mixing between neutrino flavors is assumed, so the final state leptons are either two electrons, two muons or two tau leptons. As the electron is stable and the muon is rather long-lived, both of these leptons can be detected directly. The tau lepton on the other hand decays quickly through the weak interaction, $\tau^- \to W^-\nu_\tau$, leading to a final state of missing energy from the neutrinos (which interact so weakly that they traverse the detector without leaving a trace) and additional particles from the decay of the W boson ($W^- \to l^-\nu_l$ or $W^- \to q\bar{q}$). Consequently only the final states containing electrons or muons are considered in this thesis.

In searches for heavy Majorana neutrinos and $W_R^\pm$ bosons this is in many ways a golden channel. Most important is the possibility of same sign leptons in the final state due to the Majorana nature of the heavy neutrino. While opposite sign dileptons are produced abundantly in SM processes, same sign dileptons processes are very rare. The expected sensitivity to a Majorana neutrino signal is therefore better in the same sign channel.

Another attractive aspect of this process is the absence of neutrinos in the final state. Then all of the energy in the final state is visible, and the mass of the $W_R^\pm$ boson can be reconstructed from the invariant mass of the two leptons and the two jets.

The gauge coupling of the W_R boson to the right-handed fermions is assumed to be equal to the gauge coupling of the W boson to the left-handed fermions; $g = g_L$. Then the free parameters of this process is the mass of the W_R boson, m_{W_R}, and the mass of the Majorana neutrino, m_N. In the KS process, the mass of the W_R boson can be measured from the invariant mass of the two leptons and two jets, while the mass of the Majorana neutrino can be reconstructed from the invariant mass of one of the leptons and the two jets.

There is no theoretical limit on the masses of the W_R boson and Majorana neutrino. Constraints on K and B meson mixing puts a limit on the W_R mass of $m_{W_R} > 3$ TeV [29].

A previous search performed by the ATLAS collaboration [30] excluded W_R masses of 4.7 TeV for Majorana neutrino masses of 1.2 TeV (electron channel) and 1 TeV (muon channel). The excluded Majorana neutrino masses extend to 2.9 TeV (electron channel) and 3.1 TeV (muon channel) for $m_{W_R} = 4.3$ TeV. The exclusion limit plot is shown in figure 4.2.

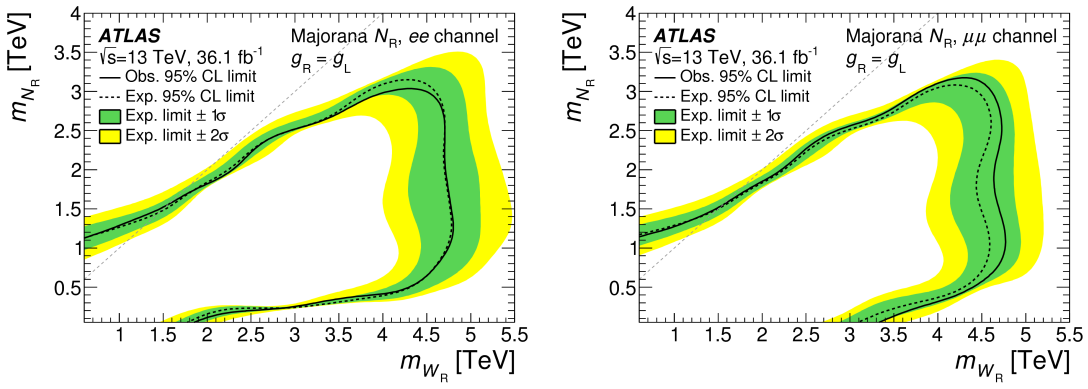

(a) $e^{\pm}e^{\pm}$ (b) $\mu^{\pm}\mu^{\pm}$

Figure 4.2: Exclusion limit plot in the $m_{W_R} - m_N$ plane at 95% CL from the recent ATLAS search [30]. The green and yellow areas correspond to respectively one and two standard deviations of the expected fluctuations of the observed limit in the absence of a signal.

Chapter 5

Production

5.1 Kinematics of particle collisions

Particles are created when other particles interact. As energy can be converted to mass as given by Einsteins famous formula $E = mc^2$ [31], heavier particles can be produced when high energy particles collide. The W_R boson and the Majorana neutrino are too heavy to exist at our energy level, but (if they exist) can be produced in particle collisions.

The kinematics of a particle are described by its energy E and its three-momentum $\vec{p} = (p_x, p_y, p_z)$. Together they form the four-momentum $P^\mu = (E, \vec{p})$. The energy and three-momentum are related by the energy-momentum formula

$$E = \sqrt{m^2 + \vec{p}^2} \tag{5.1}$$

where m is the rest mass of the particle.

The four-momentum squared

$$P^2 = P^\mu P_\mu = E^2 - \vec{p}^2 = m^2 \tag{5.2}$$

is a useful quantity because it is Lorentz invariant and conserved.

Let us consider two particles colliding and producing a new particle. The initial particles have four-momentum $P_1^\mu = (E_1, \vec{p}_1)$ and $P_2^\mu = (E_2, \vec{p}_2)$, while the final particle has four-momentum $P_3^\mu = (E_3, \vec{p}_3)$. The center of mass (CoM) of the system is defined as the frame where the total three momentum of the system is zero, which implies

$$\vec{p}_2 = -\vec{p}_1 \tag{5.3}$$

in the CoM. Then the initial four-momentum is

$$P^\mu = (E_1 + E_2, \vec{p}_1 - \vec{p}_1) = (E_1 + E_2, 0) \tag{5.4}$$

and the initial four-momentum squared becomes

$$P^2 = (E_1 + E_2)^2 \equiv s \tag{5.5}$$

where the Mandelstam variable s, corresponding to the total CoM energy squared, has been defined.

The four-momentum squared is conserved, so the four-momentum of the final particle must satisfy $P_3^2 = s$, which implies

$$s = m^2$$

So the heaviest particle that can be produced in a particle collision has mass $m = \sqrt{s}$, where s is the CoM energy of the colliding particles.

If a particle decays to N particles, the invariant mass of the initial particle is given by

$$m = \sqrt{(E_1 + E_2 + \cdots + E_N)^2 - (\vec{p}_1 + \vec{p}_2 + \cdots + \vec{p}_N)^2} \tag{5.6}$$

The mass of the W_R boson can be reconstructed from the invariant mass of the two leptons and and two jets

$$m = \sqrt{(E_{l_1} + E_{l_2} + E_{j_1} + E_{j_2})^2 - (\vec{p}_{l_1} + \vec{p}_{l_2} + \vec{p}_{j_1} + \vec{p}_{j_2})^2} \equiv m_{lljj} \tag{5.7}$$

Additionally the invariant mass of the two leptons m_{ll} and of the two jets m_{jj} are used in this analysis. The expressions for m_{ll} and m_{jj} are given be removing respectively all terms involving jets and all terms involving leptons from (5.7).

Working in a plane transverse to the direction of the initial particles is often useful as the initial momentum in this direction is zero. If the direction of the initial particles is defined to be along the z-axis in a cartesian coordinate system, the transverse momentum p_T is defined as the component of the momentum that is perpendicular to the z-axis

$$p_T = \sqrt{p_x^2 + p_y^2} \tag{5.8}$$

Finally the sum of transverse momenta, in this thesis referred to as H_T, is defined as

$$H_T = \sum p_T \tag{5.9}$$

5.2 Proton proton collisions at the LHC

This thesis uses data from proton-proton collisions at the LHC [32]. The LHC is a 27 km long circular accelerator located at CERN.

Proton-proton (pp) collisions are more complex than the collisions described in the last section as the proton is a composite particle made up of quarks and gluons, commonly called partons. When high energy protons collide, hard scattering processes occur between two of the partons. Each parton carries a fraction of the total proton momentum P. The distribution of momenta within the proton is expressed in terms of Parton Distribution Functions (PDFs). The PDFs give the probability of a parton of a certain flavor to carry a fraction x of the proton momentum when participating in a hard scattering process. Figure 5.1 show the PDFs for two different values of the momentum transfer Q.

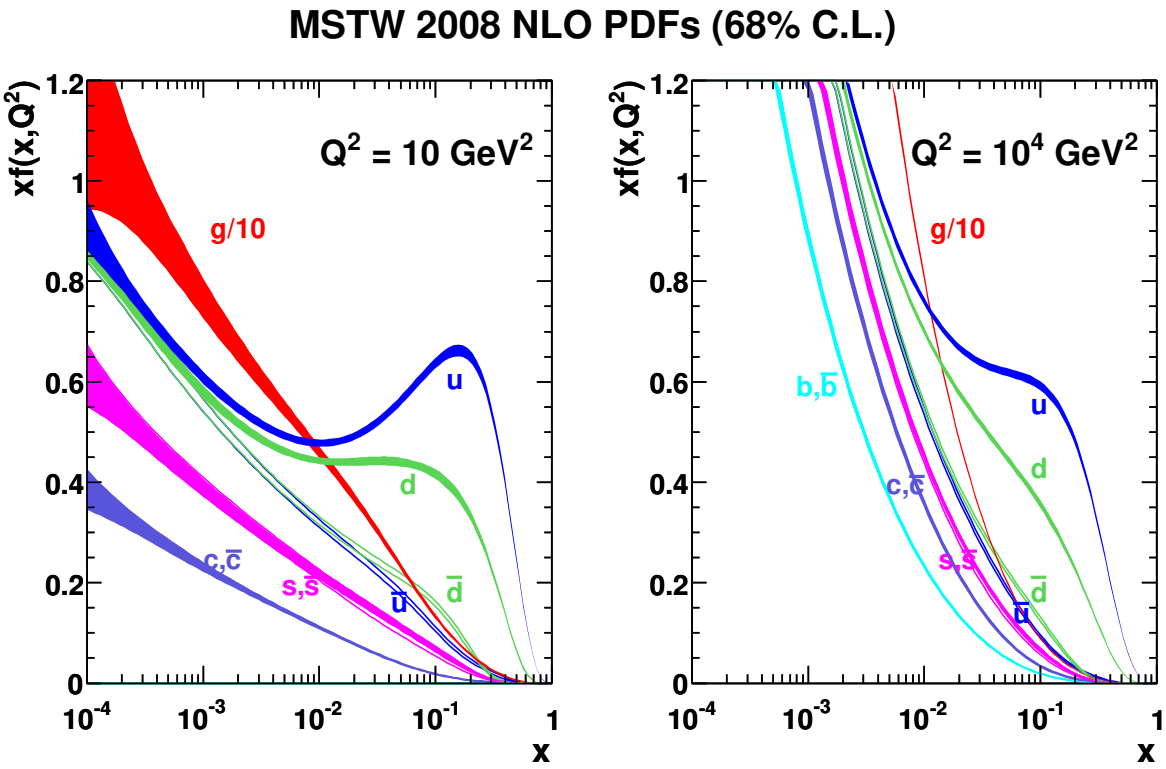

Figure 5.1: Parton distributions functions for two different values of the momentum transfer Q. The fraction of the proton momentum carried by the parton, x, is on the x-axis. The product of the momentum fraction x and the density of partons carrying the given momentum $f(x, Q^2)$ is on the y-axis. The figure is taken from [33].

The most important properties of a particle collider are its center of mass energy $\sqrt{s}$, defined in the previous section, and its luminosity, L. The luminosity is a measure of the rate of events when two particle beams collide. For a process with cross section σ, the expected number of events after a time t is given by

$$N = \sigma \int \mathcal{L}(t)\, dt \tag{5.10}$$

The luminosity integrated over time is called the integrated luminosity, and will be referred to as L.

The particles that can be produced at a particle collider depends on the the CoM energy $\sqrt{s}$, while a high luminosity is required to produce rare processes.

5.2.1 Pile-up

Because of high luminosity, more than one event can take place each time the particle beams at the LHC collide. This is known as *pile-up*. The effects of pile-up must be taken into account when reconstructing events.

5.2.2 Data samples

The data used in the main part of this analysis is from pp-collisions at the LHC in 2015 and 2016. These years were part of Run 2 at LHC, during which the accelerator was operating at a CoM energy of $\sqrt{s}$=13 TeV. The data corresponds to an integrated luminosity of $L = 36.2$ fb^{-1}.

Chapter 6

Detection

A particle can be detected through its interactions with matter. While propagating through a medium a particle interacts with other particles in the medium, either by having its direction changed by elastic collisions or by transferring energy. Charged particles interact electromagnetically, and will excite and ionize atomic electrons. Hadrons also interact strongly and emit pions (quark-antiquark pairs) in the presence of an atomic nucleus. When travelling through matter, a high energy particle leaves behind a trail of ionized electrons, photons from excitation and subsequent de-excitation of atomic electrons or jets of hadrons following the emission of a pion. As the interactions of a particle with matter depend on the properties of the particle, the particle can be identified by the manner in which it interacts. By registering the electrical signals produced by these interactions, the track of a charged particle can be reconstructed by a particle detector. In addition the energy of the particle can be measured by the amount of radiation produced in a medium when the particle's energy is completely absorbed.

For a particle to be detectable it needs to travel some distance before decaying. Thus only stable or relatively long-lived particles can be detected directly. Of the known elementary particles only the neutrinos, the electron, the proton and the photon are stable. All other particles are unstable and decay after travelling a distance of the order $\gamma v \tau$ after production, where τ is the mean lifetime of the particle and γ the Lorentz factor. The lifetime depends on the probability for the particle to decay, given by the decay rate Γ. A heavy particle generally has a shorter lifetime than a lighter one (the lifetime also depends on which interaction is responsible for the decay). Some light particles such as the muon μ and certain hadrons (kaons, pions and neutrons) can travel relatively long distances before decaying and can be detected, while heavier particles decay instantaneously.

The expected large mass of the W_R boson and the Majorana neutrino indicates a very short lifetime, and these particles will decay quickly if produced at the LHC. Thus they cannot be detected directly, and can only be discovered through the detection of their decay products. For the Keung-Senjanović process, the decay products of the W_R boson and Majorana neutrino are two same flavor leptons and two jets. The decay to tau leptons is not studied in this analysis, and the leptons considered are two electrons or two muons.

To sum up the discovery of the W_R boson and the Majorana neutrino depends on our ability to identify and reconstruct electrons, muons and jets. These particles can be reconstructed by the energy they leave behind when interacting with matter.

In this chapter the interactions of particles are discussed. The ATLAS detector and its components are then presented. Finally the reconstruction and identification of electrons, muons and jets is introduced.

6.1 Interactions of particles with matter

All charged particles interact via the electromagnetic interaction. A relativistic charged particle interacts with the atomic electrons and loses energy through ionization of atoms. The energy loss by ionization is given by the Bethe-Bloch equation [34], and increases roughly as the logarithm of the particle energy. The energy loss due to ionization is small. Hence particles with ionization as the primary mechanism for energy loss can travel a long distance before having their energy completely absorbed.

Charged particles can also lose energy through bremsstrahlung, a process in which a particle radiates a photon when deflected by the electrostatic field of a nucleus. The energy loss from bremsstrahlung increases nearly linearly with energy, making it more significant than ionization for high energy particles. The critical energy E_c is defined as the energy where the particle loses as much energy through ionization as through radiation, and bremsstrahlung accounts for the majority of the energy loss for $E > E_c$.

The probability for a particle to radiate a photon in the presence of an atomic nucleus is inversely proportional to its mass squared, $\sigma_{brems} \propto 1/m^2$, making this an important energy loss process for light particles such as the electron while it is usually negligible for muons and heavier particles. For the electron the critical energy is typically of the order of a few tens of MeV, with $E_C \approx 9.5$ MeV in lead [34]. Figure 6.1 shows the fractional energy loss per radiation length as a function of the electron energy when the electron is travelling through lead.

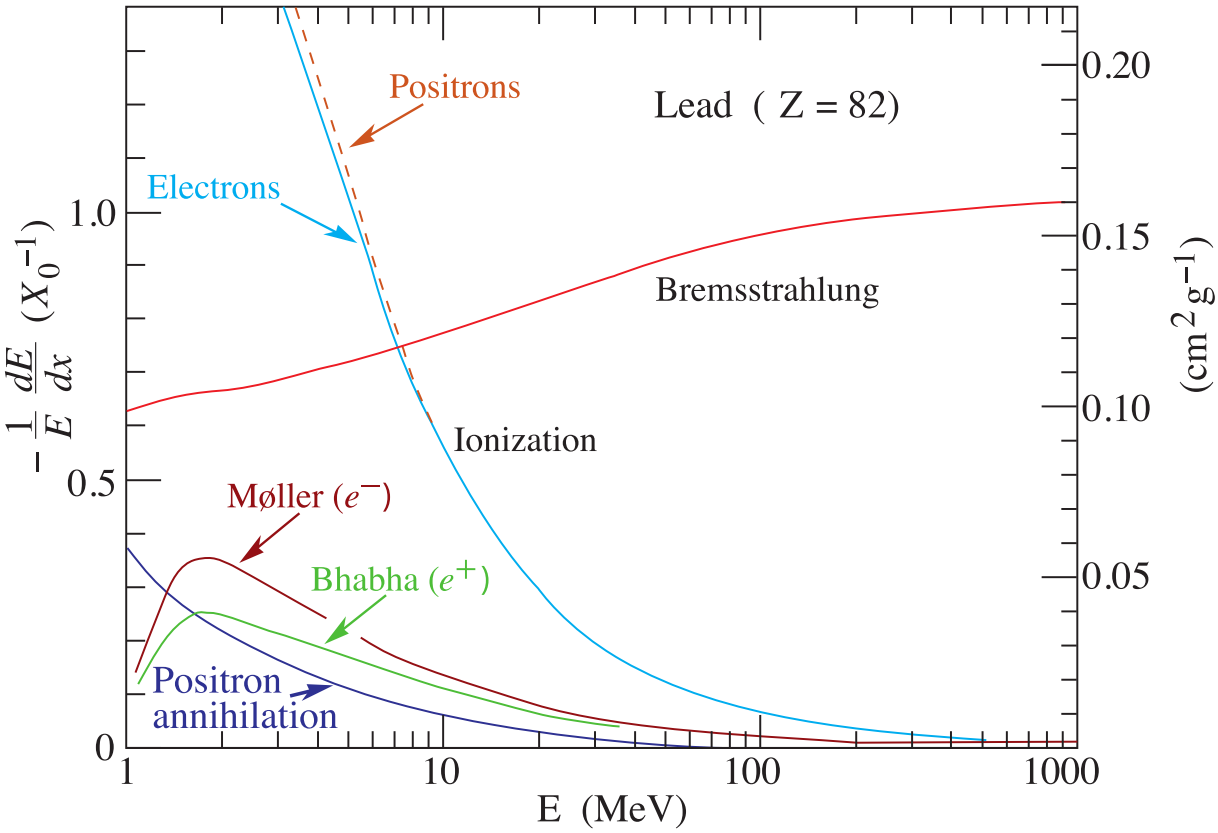

Figure 6.1: The fractional energy loss for an electron or positron in lead as a function of its energy, taken from page 453 of ref. [3].

The photon emitted by the electron can go through pair production in the presence of an atomic nucleus Z, a process in which the photon materializes as an electron and a positron, $\gamma + Z \to Z + e^+ + e^-$. As the electron and positron can again radiate a photon, an electron (or positron) with energy above the critical energy produces an electromagnetic shower when propagating in a medium as more and more particles are produced through bremsstrahlung and subsequent pair production. An illustration of an electromagnetic shower initiated by a photon is shown in fig 6.2.

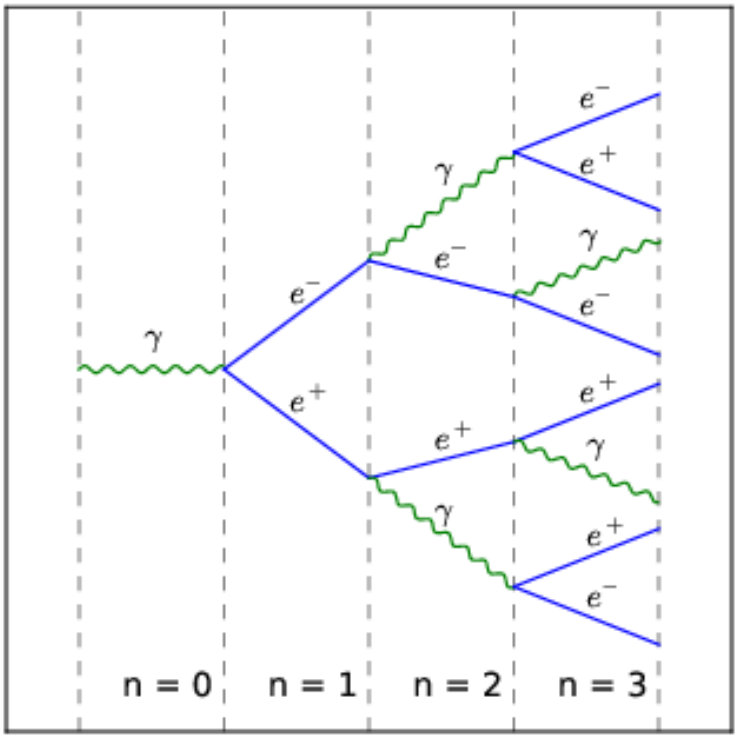

Figure 6.2: An illustration of an electromagnetic shower, taken from [35]. In this illustration the shower is initiated by a photon. n denotes the number of radiation lengths, which is the average length travelled in a medium before the initial energy has been reduced by a factor $1/e$ due to bremsstrahlung.

The radiation length X_0 is the length travelled before the initial energy E_0 of an electron is reduced by a factor $1/e$ due to bremsstrahlung, where e is the base of the natural log. The energies of the produced electrons and positrons decreases rapidly as the number of produced particles increases, with an average energy after x radiation lengths of [36]

$$\langle E \rangle \approx \frac{E}{2^x} \tag{6.1}$$

Ultimately the produced electrons and positrons reach a value below the critical energy, at which point the particles lose energy mostly through ionization. In lead, which has a radiation length of about 0.56 cm [36], the shower initiated by a 100 GeV electron will reach the critical energy after about 13 radiation length. This corresponds to less than 10 cm of material. As the energy loss due to radiation is a quick process, the initial energy of the electron is absorbed in a small volume. The total energy of the primary electron can e.g. be reconstructed by measuring the ionization from the electrons in the shower in an electromagnetic calorimeter.

For muons ionization is the main source of energy loss, making them highly penetrating. Tracking chambers specially dedicated to muons are required to reconstruct the kinematic properties of the muon.

All hadrons interact through the strong interaction by emission of a quark-anti quark pair. When propagating in matter the hadronic parts of a jet produces a cascade of

particles, much like an electromagnetic shower. The hadronic shower is less uniform than the electromagnetic shower as a wider range of particles can be created through the strong interaction. In addition the shower may also include electromagnetic parts as any produced neutral pion decay to two photons, $\pi^0 \to \gamma\gamma$, with a branching ratio of about 98.8% [3]. The energy of the jet can be measured in a hadronic calorimeter, which consists of a high density material to ensure a high rate of strong interaction processes.

Electrons, muons and jets leave different signals when travelling through a medium, making their identification and reconstruction possible with a particle detector. The ATLAS detector at CERN is designed to gather as much information as possible from the particle collisions at the LHC. Figure 6.3 illustrates how different particles leave signals in the ATLAS detector.

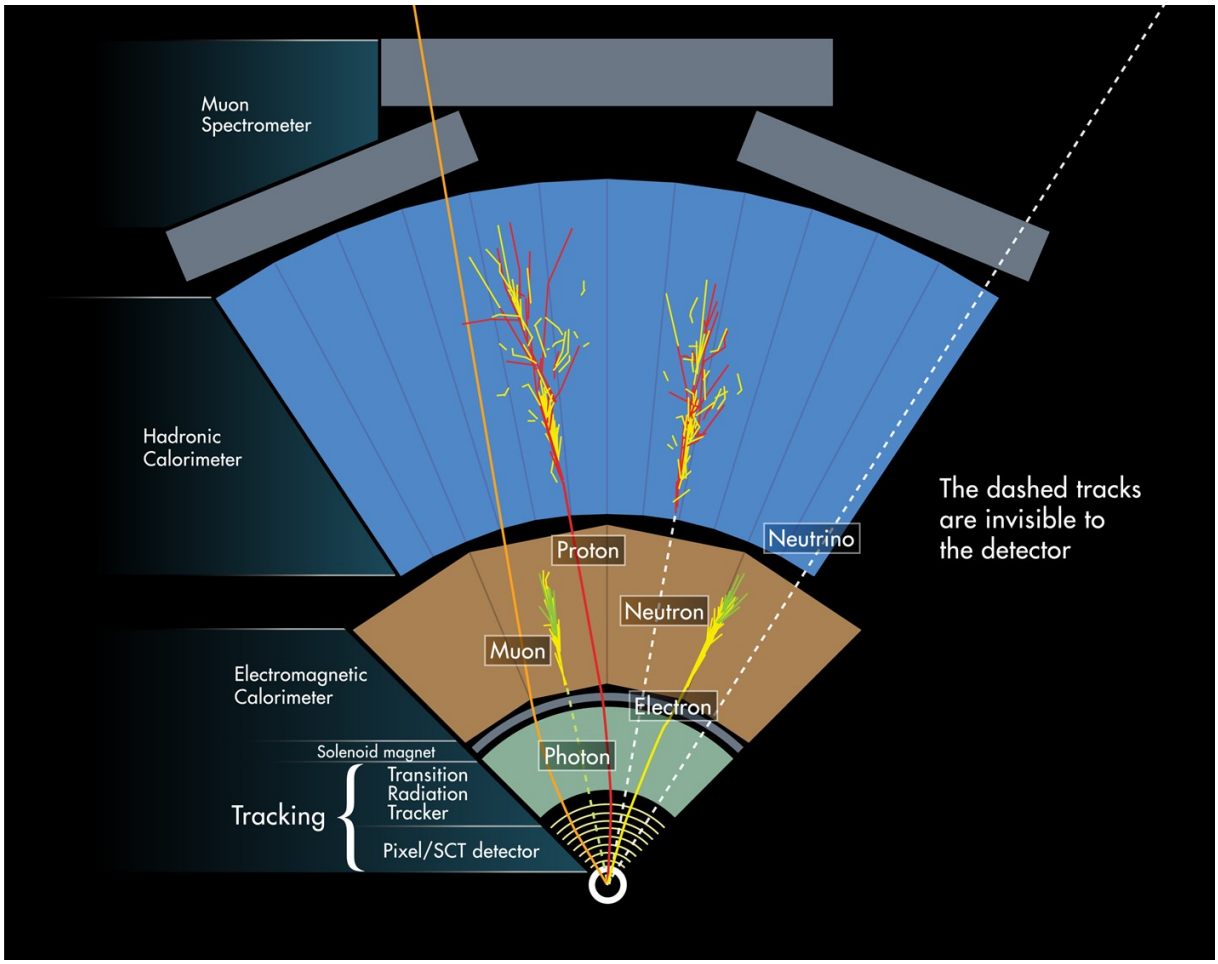

Figure 6.3: An illustration of how different particles leave signals in the ATLAS detector, taken from [37]. All charged particles will leave signals in the tracking chambers, and their track will be curved by the magnetic field. The energy of the electron is absorbed in the electromagnetic calorimeter and the jet energy is absorbed in the hadronic calorimeter. Muons traverse both the calorimeters and leave signals in the muon spectrometer.

6.2 The ATLAS detector

This thesis uses data collected by the ATLAS detector (A Toroidal LHC ApparatuS) [38], which has a cylindrical geometry and is forward-backward symmetric. ATLAS uses a cartesian coordinate system with origin at the interaction point. The z-axis is defined to be in the beam direction, while the x-axis points towards the center of the accelerator circle and the y-axis points upwards. In addition a spherical coordinate system is defined with the azimuthal angle ϕ in the xy-plane, along the beam, and the polar angle θ as the angle from the beam, with the z-axis corresponding to $\theta = 0$ and the y-axis at $\theta = \pi/2$. A useful quantity is the pseudorapidity η, defined as $\eta \equiv -\ln \tan \theta/2$. The distance between two particles is expressed in terms of their separation in the ϕ-η-plane, through $\Delta R = \sqrt{\Delta\eta^2 + \Delta\phi^2}$.

The main components of the detector are the inner detector (ID), which is surrounded by a superconducting solenoid generating a 2 T magnetic field, the electromagnetic and hadronic calorimeters and the muon spectrometer. A short review of the detector parts is given here. More details can be found in ref. [38].

A schematic view of the ATLAS detector is shown in figure 6.4.

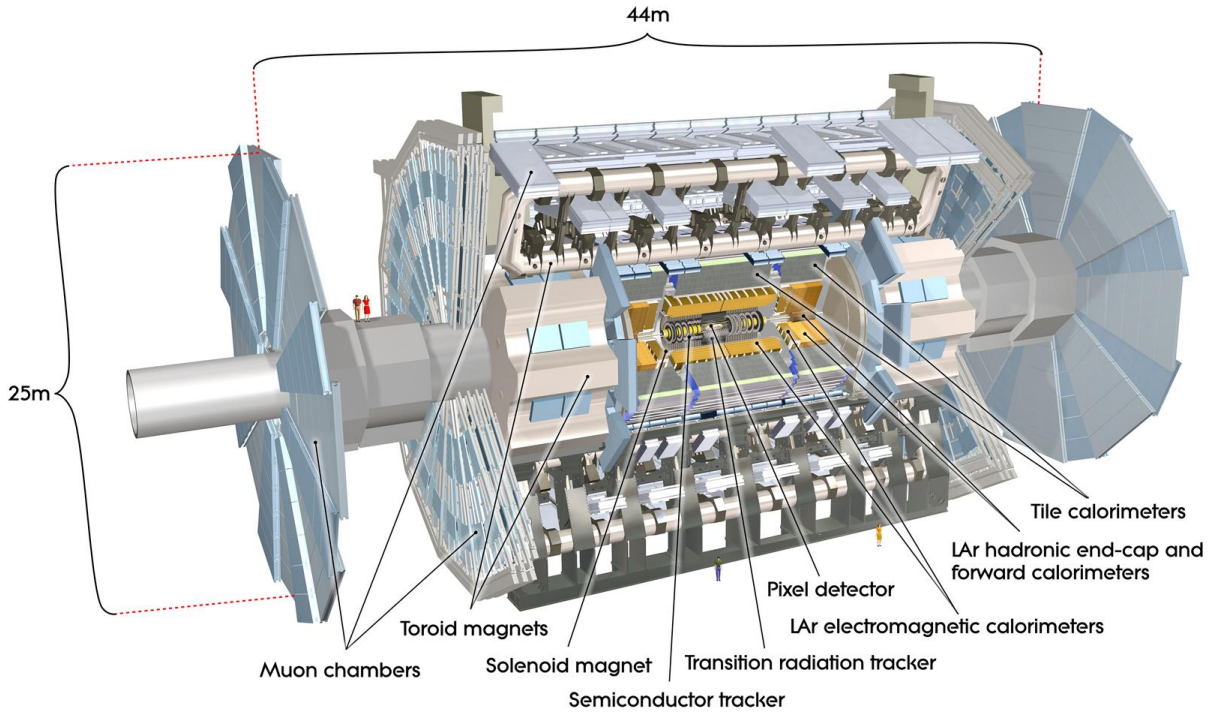

Figure 6.4: The ATLAS detector, taken from [39].

6.2.1 Inner detector

Particle tracks and interaction vertices are reconstructed in the inner detector, which is immersed in a 2 T magnetic field. A silicon pixel detector and the semiconductor tracker (SCT) cover the range $|\eta| < 2.5$. The trajectories of charged particles are bent

in the magnetic field, and the electric charge can be determined from the direction of the curvature. In addition the momentum of the particle is measured by the degree of curvature, with a required resolution of $\sigma_{p_T}/p_T = 0.05\% p_T[\text{GeV}] \oplus 1\%$ where σ_{p_T} is the resolution in the measurement of the transverse momentum and the notation $a \oplus b = \sqrt{a^2 + b^2}$ has been used to indicate that the numbers are added in quadrature.

The outermost part of the inner detector is the Transition Radiation Tracker (TRT), which extends to $|\eta| = 2$. The gas filled drift tubes of the TRT provide electron identification for a wide range of energies.

6.2.2 Calorimeters

The energy of charged particles and hadrons is measured in the calorimeters, which cover the range $|\eta| < 4.9$. Closest to the interaction point is the electromagnetic calorimeter (ECal), where the energy of photons and electrons is absorbed. Lead is used as the absorbing material while the energy is measured by the ionisation of liquid argon. The region $|\eta| < 1.5$ of the EM calorimeter is the barrel region, while the end-cap regions cover the range $1.37 < |\eta| < 3.2$. In the transition region between the barrel and the end-cap, the so-called crack region, there is a larger uncertainty in the reconstruction of electrons and photons. Electrons from this region are not included in the analysis. The EM calorimeter offers high precision in the measurement of the energy, with $\sigma_E/E = 10\%/\sqrt{E[\text{GeV}]} \oplus 0.7\%$ as the design resolution for $|\eta| < 3.2$.

The hadronic calorimeter (HadCal) measures the energy of strongly interacting particles, using scintillating tiles as the active detector material and steel as the absorbing material. Due to the more complex nature of the hadronic shower, the precision is not as good as for the EM calorimeter. In the HadCal the resolution is $\sigma_E/E = 50\%/\sqrt{E[\text{GeV}]} \oplus 3\%$ in the barrel and end-cap regions ($|\eta| < 3.2$).

In addition to the barrel and end-cap regions, the Forward LAr Calorimeters (FCal) covers the region $3.1 < |\eta| < 4.9$. The FCal include both an electromagnetic and a hadronic part. The required resolution in the forward region is $\sigma_E/E = 100\%/\sqrt{E[\text{GeV}]} \oplus 10\%$, which is adequate for the measurement of jet energies and missing energy.

6.2.3 Muon spectrometer

The outermost part of the detector is the muon spectrometer (MS), which contains separate triggers and tracking chambers. Three air-core toroids provide a magnetic field that enables the measurement of the muon momentum and electric charge. Three layers of precision chambers cover the range $|\eta| < 2.7$ and provide excellent resolution in the reconstruction of the muon momentum. The required resolution is $\sigma_{p_T}/p_T = 10\%$ at p_T =1 TeV.

6.2.4 Trigger system

Events of interest are selected only using a three level trigger system [40], which reduces the amount of stored data. Based on information from the detector, the hardware Level-

1 (L1) trigger makes quick decisions about which events to store. The software-based Level-2 (L2) trigger and event filter form the high-level trigger (HLT), which puts additional requirements on the kinematic properties of the reconstructed objects using refined detector information and algorithms. All events passing both the L1 and HLT are stored for offline processing.

6.3 Object definitions and event selection

The signals from the different components of the ATLAS detector are used to identify the final state particle candidates of the event and reconstruct their tracks and kinematic properties. This process, where objects are constructed from the detector signals, is known as event reconstruction. When reconstructing an event, the following parameters are important:

- d_0 - the transverse impact parameter, defined as the shortest distance between the reconstructed particle and the beam line in the transverse direction.
- z_0 - the longitudinal impact parameter, defined as the shortest distance between the reconstructed particle and the primary vertex in the longitudinal direction.

The particles of interest are the ones that originate from the primary vertex. These particles are denoted *signal* or *prompt*. Both electrons and muons can be produced by semileptonic in-flight decay of hadrons in the ID. In addition jets can mimic the signals of a charged lepton and electrons can be produced from photon conversions. These uninteresting leptons are known as *background* leptons. To differentiate between background and signal leptons, requirements are made on their properties. These requirements are made to optimize the selection efficiency of signal leptons while maintaining a high rejection efficiency for background leptons. Furthermore hard jets must be distinguished from pile up jets.

6.3.1 Electrons

Being a charged light particle, the electron leaves a signal in the ID before having its energy absorbed in the ECal by initiating an electromagnetic shower. An electron candidate is reconstructed by matching the cluster in the EMCal to a track in the ID, which distinguishes it from the clusters caused by a photon as the electrically neutral photon does not leave signals in the ID. As electrons can be produced in the detector through semileptonic hadron decays and through photon conversions, several requirements are made to differentiate these background electrons from the more interesting signal electrons originating from the main decay.

The signal electrons selected for this analysis satisfy $E_T > 30$ GeV and are required to fall within the pseudorapidity region $|\eta| < 2.47$. Any electron in the crack region ($1.37 < |\eta| < 1.52$) is excluded. They are identified using a likelihood-based (LH) identification, which combines information from the ID and the calorimeter to calculate the probability for the electron to be signal or background [41]. An electron identification working point of LHMedium, which has a prompt electron identification efficiency of about 88% for

electrons with $E_T = 40$ GeV [42] and good rejection of background electrons, is used in this analysis.

To further separate the signal electrons from background electrons, requirements are made on the isolation of the electron. The track of a background electron is often surrounded by other particles, while a signal electron can be recognized by an absence of activity in its vicinity. To quantify the amount of activity in the proximity of the electron, a cone with radius $\Delta R = 0.2$ is defined around the electron candidate. The isolation operating point Gradient is used in this analysis, providing an isolation efficiency $\epsilon_{iso} = 90(99)\%$ at 25(60) GeV.

6.3.2 Muons

Muons leave signals in the ID and the MS, as well as energy deposits in the calorimeters corresponding to a minimum ionizing particle. As muons are the only visible particles that penetrate the detector calorimeters, a muon candidate is identified by hits in the MS. If the signals in the MS have matching tracks in the ID, the muon is called *combined (CB)*. The ID cover the region $|\eta| < 2.5$, so the region $2.5 < |\eta| < 2.7$ of the MS is not covered by the ID. Hence muons reconstructed in this pseudorapidity region cannot be matched to a track in the ID. Such muons are called *extrapolated (ME)*.

The muons selected for this analysis are required to be combined, and thus must fall within the pseudorapidity region $|\eta| < 2.5$. All selected signal muons satisfy $p_T > 30$ GeV. The Medium identification operating point is used for the selection of signal muons and rejection of background muons, which mainly originate from in-flight hadron decay. For high momentum ($20 < p_T < 100$ GeV) the medium identification provides a signal muon selection efficiency of 96.1 % and a hadron selection efficiency of 0.17 % [43].

The isolation working point FixedCutTightTrackOnly is chosen for the muons. A muon satisfies the chosen isolation if $p_T^{\text{varcone30}}/p_T^{\mu} < 0.06$ [43], where p_T^{μ} is the transverse momentum of the muon and $p_T^{\text{varcone30}}$ is the the sum of all transverse momenta in a cone of $\Delta R = 10\text{ GeV}/p_T^{\mu}$ around the muon, with ΔR required to be less than 0.3.

The definition of signal electrons and muons is summarized in table 6.1.

Table 6.1: Summary of the object definitions for signal electrons and muons.

Channel	$e^{\pm}e^{\pm}$	$\mu^{\pm}\mu^{\pm}$
Identification	LHMedium	Medium
Isolation	Gradient	FCTightTrackOnly
p_T	$p_T > 30$ GeV	$p_T > 30$ GeV
η	$\lvert\eta\rvert < 2.47$ and veto $1.37 < \lvert\eta\rvert < 1.52$	$\lvert\eta\rvert < 2.5$
$\lvert d_0\rvert/\sigma_{d_0}$	$\lvert d_0\rvert/\sigma_{d_0} < 5$	$\lvert d_0\rvert/\sigma_{d_0} < 3$
$\lvert z_0 \sin\theta\rvert$	$\lvert z_0 \sin\theta\rvert < 0.5$ mm	$\lvert z_0 \sin\theta\rvert < 0.5$ mm

6.3.3 Jets

Jets are reconstructed with the anti-k$_t$ algorithm [44] using a radius parameter of $R = 0.4$. The algorithm takes the calorimeter energy deposits as input [45]. Central jets, which

fall within the region $|\eta| < 2.5$, are used in this analysis. The reconstructed central jets are required to satisfy $p_T > 20$ GeV. Jets from pileup are suppressed using the jet-vertex-tagger (JVT) [46].

Rejection of events containing b-jets is useful to suppress background from processes with top quarks. The b-jets are quite rather long lived and produce a secondary vertex, which is used to tag the b-jets [47]. The MV2c10 b-jet tagging algorithm is used in this analysis, with a 77 % tagging efficiency.

6.3.4 Triggers

The selected leptons are required to pass one of HLT dilepton triggers given in table 6.2. All selected triggers where unprescaled during the data taking periods [48].

Year	Trigger OR
2015	2e12_lhloose_L12EM10VH, 2mu10
2016	e17_lhloose_nod0_2e9_lhloose_nod0, 2e17_lhvloose_nod0, 2mu10, 2mu14
2017	2e17_lhvloose_nod, 2e24_lhvloose_nod0, mu22_mu8_noL1, 2mu14

Table 6.2: Dielectron and dimuon triggers used in this analysis.

Part III

Analysis

Chapter 7

Analysis procedure

When searching for new particles, what we wish to observe is events in the data matching the signature of the particles in question. For the Keung-Senjanović process, the signature of Majorana neutrino and W_R production is two same sign same flavor leptons and (at least) two jets. When searching for these particles, events that match this signature are selected from the data. Additional requirements are made on the properties of the final-state particles, and the events that meet these criteria are counted.

Observing events that satisfy these criteria does not automatically imply that a Majorana neutrino and a W_R boson were produced at the LHC. The final state particles could just as well be the products of the production of a Z boson, a W boson or some other SM particle. To discover a new particle it is not sufficient to observe events that match the signature of the particle. What we need to observe is an excess in the number of data events, i.e. more events than what is expected from the current background predictions. The first step in this process is to understand and simulate the SM background.

In this chapter the simulated MC background and signal samples are introduced. The first distributions of preselected events are then shown, and truth classification is used to better understand the different sources of background. Finally the SM processes contributing to the background are discussed.

7.1 Background simulation

The SM background is simulated using Monte Carlo (MC) event generators. A framework based on GEANT4 [49] mimics the response of the ATLAS detector to the different background events. The MC generators used for the background simulation in this thesis are Sherpa [50], Pythia [51] and Powheg [52]. The generators and parton distribution functions (PDFs) used for the different physics processes and are summarized in table 7.1.

Process	MC Generator	PDF
Diboson	SHERPA	NNPDF3.0NNLO
Z+jets	SHERPA	NNPDF3.0NNLO
W+jets	SHERPA	NNPDF3.0NNLO
$t\bar{t}$	POWHEG + PYTHIA	NNPDF3.0NLO
Single Top	POWHEG + PYTHIA	NNPDF3.0NLO
$t\bar{t}V$	PYTHIA	NNPDF2.3LO

Table 7.1: Simulated background samples.

7.2 Signal samples

Signal samples were simulated using the PYTHIA and MADGRAPH[53] generators. Simulated samples for a range of W_R and N_R masses were used in this analysis. The signal grid is shown in table 7.2.

m_{W_R} [GeV]	m_{N_R} [GeV]
3000	100
3600	900, 1800, 2700, 3500
4000	100
4200	1050, 2100, 3150, 4100
4500	100, 600, 800, 1000, 1500, 2000, 2250, 3375, 4400
5000	100, 600, 800, 1000, 1500, 2000, 2500, 3750, 4900
6000	100, 800, 1000, 1500, 2000

Table 7.2: The grid of simulated W_R and N_R masses used in this analysis.

7.3 Preselection and a first study of the background

As a first selection, events with at least two jets and two same flavor leptons that pass the selected triggers in tab 6.2 are chosen. To motivate the study of the same sign channel, events with both same sign and opposite sign leptons are selected and plotted separately.

The resulting distributions of the invariant mass of the two leptons and two highest p_T jets are shown in figure 7.1. The upper part of the plots shows the expected number of background and signal events as a function of m_{lljj}. Two signal samples, one with $m_{W_R} = 3.6$ TeV and $m_{N_R} = 1.8$ TeV and another with $m_{W_R} = 4.2$ TeV and $m_{N_R} = 1.05$ TeV, are included for illustration. The total number of expected background, the expected number of signal events and the contribution from the different MC samples to the total background in percentage are indicated by the numbers in parentheses.

The lower part of the plots show the expected significance Z of the signal when integrated from the given bin and to the right. The expected significance quantifies the separation between background and signal. A high expected significance implies good sensitivity to the signal, and is therefore desirable when searching for new particles. The expected significance will be introduced in more detail in the next chapter.

The search is performed in the $e^{\pm}e^{\pm}$ and $\mu^{\pm}\mu^{\pm}$ channels independently as there is no theoretical requirement for the masses of the N_e and N_μ to be equal. Additionally the background and sensitivity is different between the two channels.

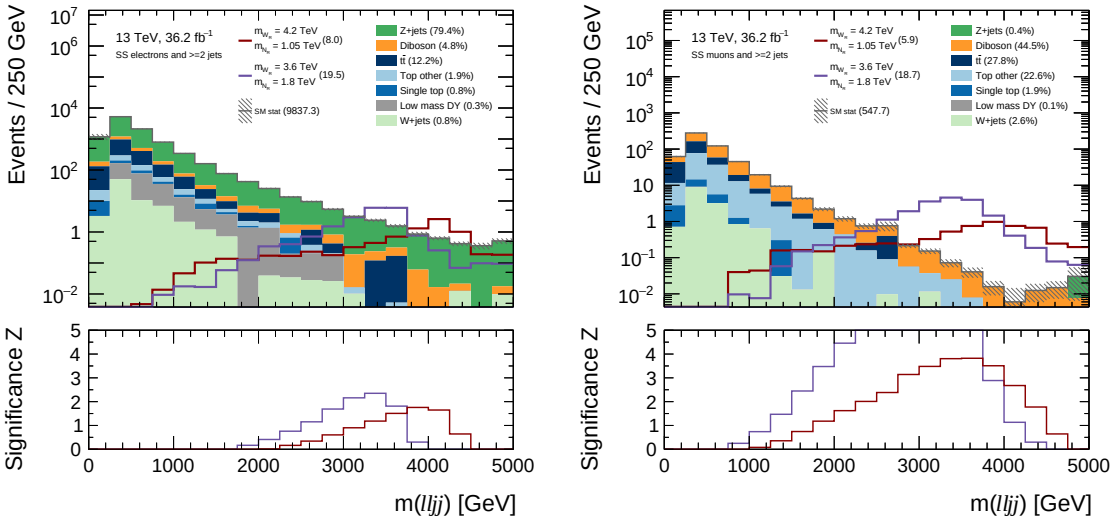

(a) $e^{\pm}e^{\pm}$

(b) $\mu^{\pm}\mu^{\pm}$

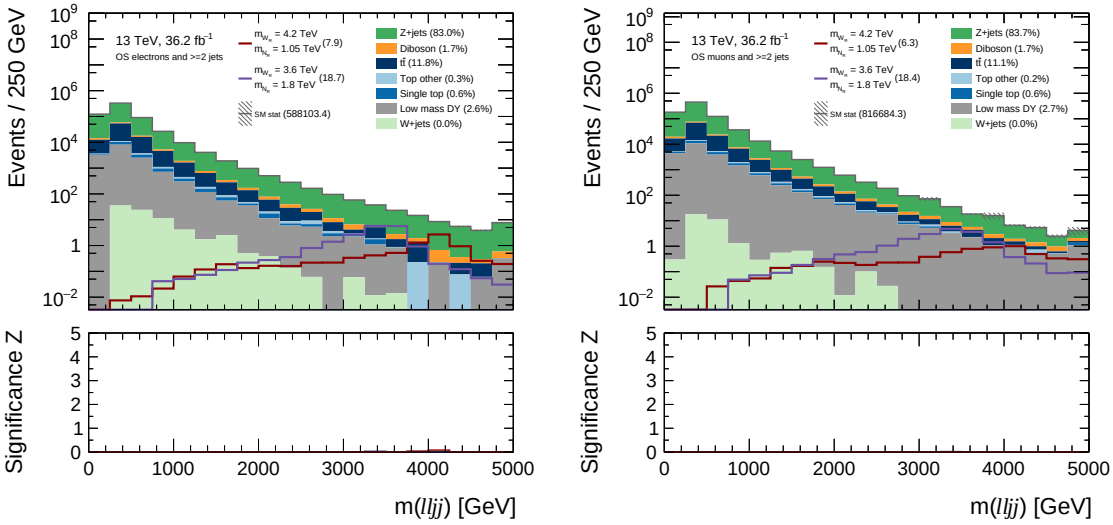

(c) $e^{\pm}e^{\mp}$

(d) $\mu^{\pm}\mu^{\mp}$

Figure 7.1: Distribution of m_{lljj}, the invariant mass of the two leptons and two highest p_T jets, for events with at least two jets and (a) two same sign electrons, (b) two same sign muons, (c) two opposite sign electrons and (d) two opposite sign muons.

The distributions in figure 7.1 clearly justify focusing on the same sign channel, as the expected background for opposite sign leptons is several orders of magnitude larger than the that expected for same sign leptons. By choosing same sign leptons the expected significance is already quite high before imposing any further cuts, especially in the muon channel. For the opposite sign leptons the large background completely drowns the signal, which necessitates an elaborate set of cuts to make the search sensitive to the signal.

Another thing to notice is the contributions to the background in the same sign channel. The background in the electron channel is $\sim$ 10 times larger than the background in

the muon channel, with the main contribution to the background coming from Z+jets processes. A Z boson decaying leptonically produces leptons with opposite sign, $Z \rightarrow l^+l^-$, due to conservation of charge and lepton number, and should in theory not contribute to the same sign background. Processes that produce only one prompt lepton, such as W+jets and certain top processes, also have a non-zero expected number of events in both channels. To better understand the same sign background, the next section focuses on using the truth information to classify the different sources of background.

7.4 Truth classification

The truth information in the MC samples can be used to classify the background according to the source it stems from. When the background is simulated using MC generators, particles are separated into truth particles and reconstructed particles. The reconstructed particles are the objects identified by the simulated ATLAS detector, while the truth particles are the ones that were actually produced. By comparing the truth information to the information about the reconstructed particle, the origin of the reconstructed particle can be determined.

The sources of background are identified using the MCTruthClassifier tool [54], which defines the type and origin of the particles. Based on the truth information, the sources of background can be divided into categories based on the true origin of the reconstructed leptons:

- Prompt - real leptons that originate from the decay of a top quark or Z, W or H bosons.
- Charge flip - prompt leptons that are reconstructed with the wrong charge.
- Photon conversion - leptons produced when an emitted photon undergoes pair production.
- Heavy flavor - non-prompt leptons from decays inside heavy flavor (c or b) jets or heavy flavor jets being misidentified as leptons (fake leptons).
- Light flavor - leptons from decays inside light flavor jets or light flavor jets being misidentified as leptons (fake leptons).

The truth information should not be trusted blindly as it primarily gives information about how the generator models the detector, and not about the detector itself. It can still give a good indication of the different sources of background. The distributions of the invariant mass of the two leptons and two leading jets with the background classified based on the truth information are shown in figure 7.2. Unclassified leptons are not included in the distributions, so the number of events in figure 7.2 is a slightly smaller than in 7.1.

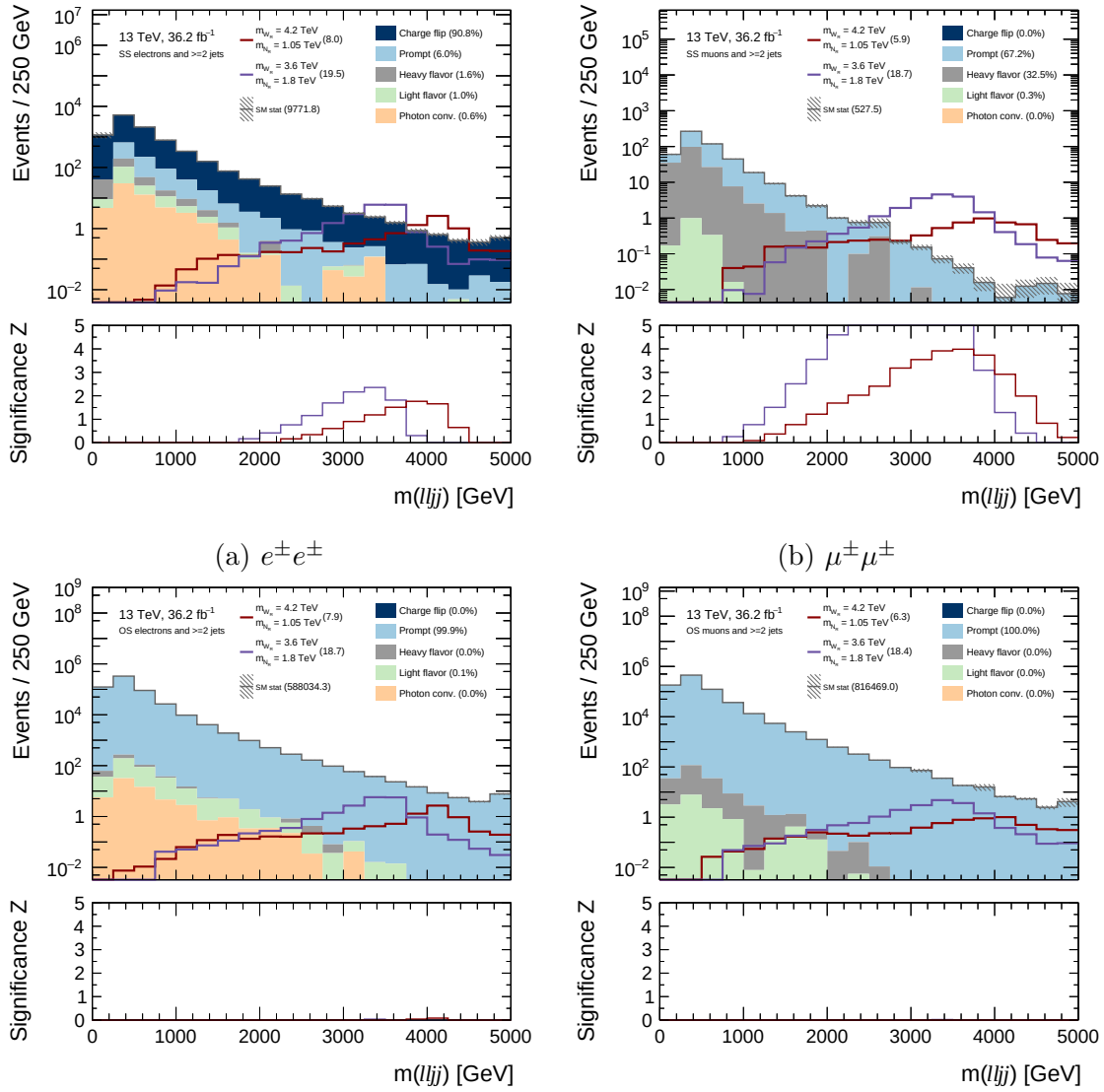

(a) $e^{\pm}e^{\pm}$ (b) $\mu^{\pm}\mu^{\pm}$

(c) $e^{\pm}e^{\mp}$ (d) $\mu^{\pm}\mu^{\mp}$

Figure 7.2: Distribution of m_{lljj}, the invariant mass of the two leptons and two highest p_T jets, for events with at least two jets and (a) two same sign electrons, (b) two same sign muons, (c) two opposite sign electrons and (d) two opposite sign muons. The sources of background are classified using the truth information. Leptons that have for some reason not been classified by the MCTruthClassifier tool have not been included in the distributions. Hence the total number of events is a little smaller than in figure 7.1.

As the background from SM processes is large in the OS channel, prompt leptons dominate the contribution to the background in this channel. But as the expected SM background in the SS channel is small, the contribution from non-prompt and fake leptons is significant. In the electron channel most of the background is classified as charge flip, which means one of the electrons has been identified with the wrong charge. The charge flip background is the subject of section 9.2, and is reduced using the Charge Flip ID Selector tool [55].

Non-prompt leptons from decays within jets, photon conversions and misidentified (fake) leptons will from this point onward collectively be referred to as "fakes". Fakes are generally not well modelled by the MC simulations, and are hereafter estimated using the

data-driven matrix method. More details are presented in section 9.3. To avoid double counting of fake background events, the truth information is used to only include prompt and charge flip leptons from the MC simulations.

The distributions of the invariant mass of the two leptons and two leading jets after charge flip reduction and fake estimation are shown in figure 7.3. Notice the clear reduction of background in the electron channel.

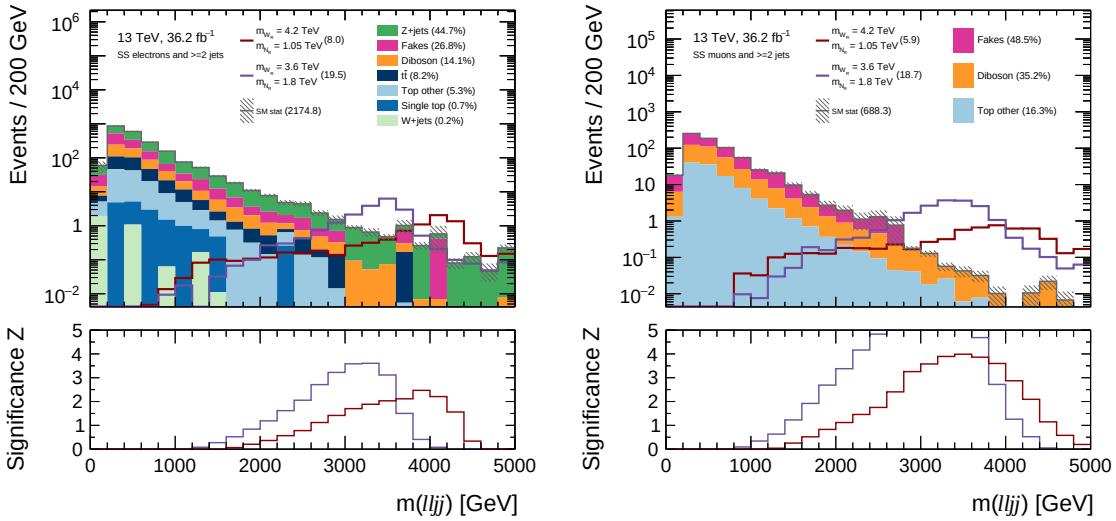

(a) $e^{\pm}e^{\pm}$ (b) $\mu^{\pm}\mu^{\pm}$

Figure 7.3: Distribution of the invariant mass of the two leptons and two leading jets, m_{lljj}, after charge flip reduction and data-driven fakes estimation. The last bin contains the overflow.

After requiring prompt leptons in the MC, certain background samples have zero contribution in the $\mu^{\pm}\mu^{\pm}$ channel. For simplicity these processes will not be included in the following plots.

7.5 Standard Model backgrounds

7.5.1 Prompt

As a result of lepton number conservation, there is no process in the Standard Model that leads to a final state of exactly two same sign leptons. We can however get contributions to the prompt background from processes which produce three or more charged leptons if the "extra" leptons are not reconstructed. Examples of such processes are the production and decay of two weak gauge bosons (dibosons) or a $t\bar{t}$ pair produced in association with a W or Z boson.

Dibosons

Processes which produce either two Z bosons or one Z boson and a W boson can lead to a final state of at least three charged leptons if both bosons decay leptonically. Examples of such processes are illustrated in figure 7.4. These processes contribute to the dilepton background if only two of the charged leptons are reconstructed and pass the selection cuts. If the reconstructed leptons have the same charge, we also get contributions to the same-sign background.

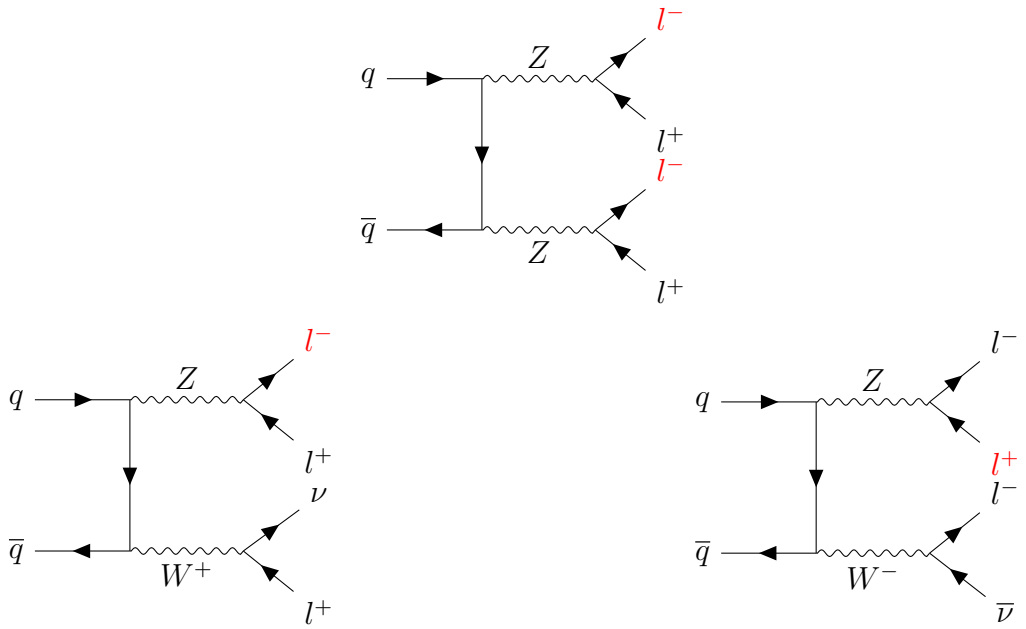

Figure 7.4: Examples of diboson production and decay in pp collisions. These processes contribute to the prompt same-sign background if the leptons marked with red color are not reconstructed (in the topmost diagram the process would also contribute if the leptons marked in red are *not* reconstructed).

Top processes

Other processes that contribute to the same sign background if one or more of the produced leptons fail the selection critera or are not reconstructed, are processes with a $t\bar{t}$ pair being produced in association with a W or Z boson. Contribution from these processes are labeled *TopOther* in the coming plots. Examples of $t\bar{t}W$ and $t\bar{t}Z$ are shown in figure 7.5.

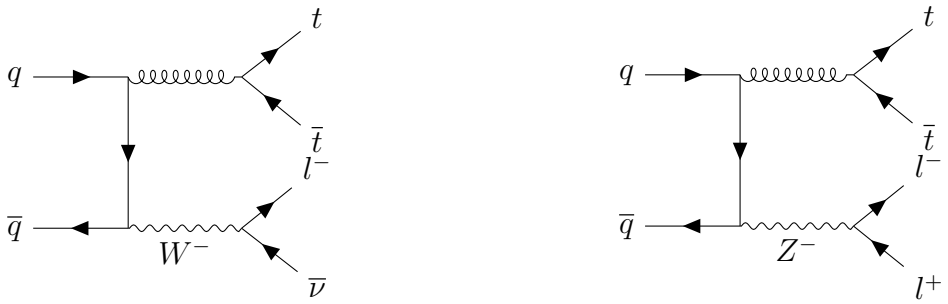

Figure 7.5: Examples of the production of $t\bar{t}W$ (left) and $t\bar{t}Z$ (right) in pp collisions.

The top quarks decay via the weak interaction, producing a b quark and a W boson. The W bosons subsequently decays either hadronically or leptonically.

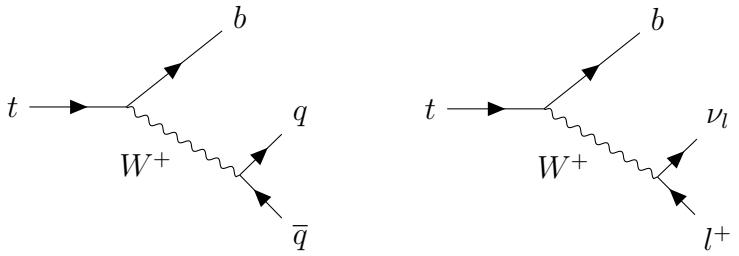

Figure 7.6: Examples of the final state produced in the decay of a top quark. The W boson either decays hadronically (left) or leptonically (right).

If both of the W bosons decay leptonically, the resulting final state has three ($t\bar{t}W$) or four ($t\bar{t}Z$) charged leptons.

7.5.2 Fakes

Processes with a final state with one prompt lepton can contribute to the SS background if one additional fake lepton is reconstructed. Examples are single top, semi-leptonic $t\bar{t}$ and W+jets. First order s-channel examples of these processes are shown in figures 7.7, 7.8 and 7.9.

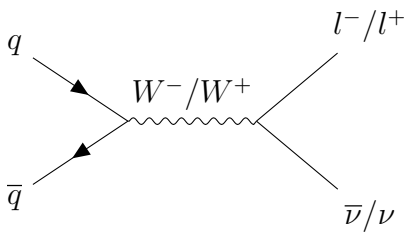

Figure 7.7: W+jets. A produced W boson can decay leptonically (as shown in this diagram) and produces a final state with one charged lepton.

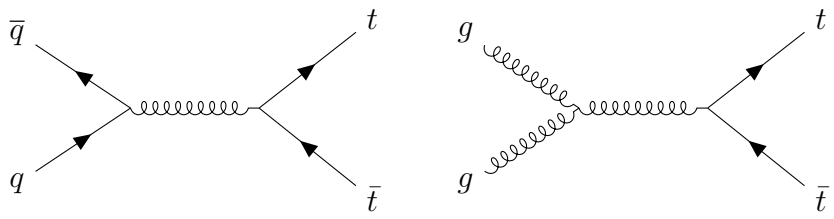

Figure 7.8: $t\bar{t}$. The top quarks decay through the weak interaction as illustrated in figure 7.6. The resulting final state has one charged lepton if one of the produced W bosons decays leptonically while the other decays hadronically.

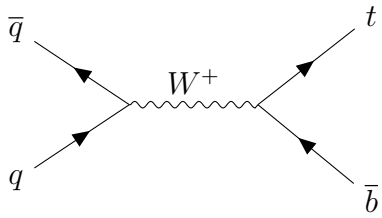

Figure 7.9: Production of a single top quark. The final state has one charged lepton if the W boson produced in the decay of the top quark decays leptonically.

The processes shown above, as well as all other processes with one prompt charged lepton in the final state or processes with several charged leptons where only one is reconstructed and passes preselection, contribute to the same sign background if one fake lepton with the same charge as the prompt lepton is reconstructed in addition.

7.5.3 Charge flip

All processes with a final state with two opposite sign leptons contribute to the charge flip background if one of the leptons has its charge misidentified.

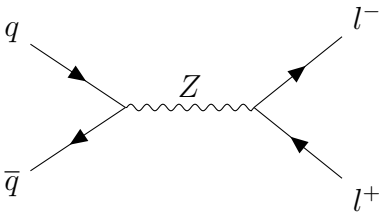

Figure 7.10: Z+jets. A Z boson decaying leptonically has a final state with two oppositely charged leptons.

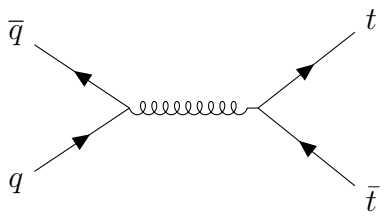

Figure 7.11: $t\bar{t}$. If both W bosons produced in the decay of the top quarks decays leptonically, this process results in a final state with two charged leptons with opposite sign.

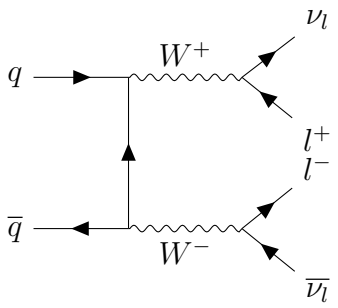

Figure 7.12: A WW process. If both W bosons decay leptonically, a final state with the oppositely charged leptons is the result.

The charge flip background is more thoroughly discussed in section 9.2.

Chapter 8

Signal event selection

Now that the same sign background is understood, further requirements can be made on the selected events to reduce the number of selected background events while keeping as many signal events as possible. The final set of cuts are known as the signal region (SR). To ensure that the SR is sensitive to the signal, studies are performed on the expected significance of the signal after applying the selected cuts.

The first part of this chapter focuses on significance and the statistical interpretation of the results. Thereafter the signal region is developed to optimize the expected significance of the signal.

8.1 Significance

To interpret the results from the coming distributions two hypotheses are formulated. The null hypothesis, H_0, is that only background SM processes contribute ("background-only" or "b-only" hypothesis). The alternative hypothesis, H_1, is that both SM and signal processes contribute to the distributions ("background+signal" or "s+b" hypothesis). If we hope to discover Majorana neutrinos and W_R bosons, our goal is to reject the b-only hypothesis.

A straight-forward way to test the hypotheses is to simply count the number of observed events. If the number of events deviates sufficiently from the expected number of events from the b-only hypothesis, we might be able to either discover the Majorana neutrino and the W_R boson or interpret the results as evidence of their presence in the data.

To determine the compatibility of the data with the b-only and s+b hypotheses, a test statistic t is constructed from the measurements. The probability of obtaining a test statistic as high or higher than the one observed under the b-only hypothesis H_0 is given by the p-value [56]

$$p = \int_{t_{obs}}^{+\infty} g(t|H_0)dt \tag{8.1}$$

A small p-value is an indication of inconsistency of the observed data with the b-only hypothesis, and $p < 2.87 \cdot 10^{-7}$ is used to claim a discovery. The p-value can also be

expressed as an observed significance, Z, defined by

$$\int_Z^\infty \frac{1}{\sqrt{2\pi}} e^{-t^2/2} dt = p \tag{8.2}$$

The significance Z is expressed in units of σ, and a p-value of $2.87 \cdot 10^{-7}$ corresponds to a significance level of 5, or 5σ.

The expected significance is the expected deviation from the b-only hypothesis assuming the s+b hypothesis to be true. The Root function NumberCountingUtils::BinomialExpZ is used for calculating the expected significance. The function takes the expected number of background events, the expected number of signal events and the background uncertainty as input to calculate Z_N [57]. Systematic uncertainties where not evaluated in this thesis. Due to few expected event and a large statistical uncertainty, systematic uncertainties do not affect the results in any considerable way. A systematic uncertainty of 40%, which is conservative in most regions, is hence used for the uncertainty.

The observed number of events is chosen as the test statistic. The observed number of events follows a Poisson distribution

$$f(n_{obs}; \nu) = \frac{\nu^{n_{obs}}}{n_{obs}!} e^{-\nu} \tag{8.3}$$

where n_{obs} is the observed number of events and ν is the expected number of events.

The p-value can then be expressed as

$$p = \sum_{t=n_{obs}}^{\infty} f(t; b - \text{only}). \tag{8.4}$$

We can evaluate the agreement between the observed number of events and the expected number of events under the b-only and s+b hypotheses by calculating the probability of obtaining an event number as small or smaller than the observed number of events under the two hypotheses. The probabilities are often expressed in terms of confidence intervals CL_b and CL_{s+b}, defined as

$$\text{CL}_b = \sum_{t=0}^{n_{obs}} f(t; b - \text{only}) \tag{8.5}$$

$$\text{CL}_{s+b} = \sum_{t=0}^{n_{obs}} f(t; s + b) \tag{8.6}$$

CL_b is the probability to obtain a number of events as small or smaller than the observed value under the b-only hypothesis, while CL_{s+b} is the probability to obtain a number of events as small or smaller than the observed value under the s+b hypothesis.

8.1.1 Exclusion

If the observed events are found to be in good agreement with the b-only hypothesis, lower limits can be set on the masses of the W_R boson and Majorana neutrino by excluding samples in the signal grid.

The CL_s technique [58] is used for exclusion, with CL_s defined as

$$CL_s = \frac{CL_{s+b}}{CL_b} \tag{8.7}$$

The signal is excluded at 95 % confidence level if $CL_s < 0.05$.

If no events are observed, three expected signal events are required for exclusion [59].

8.2 Signal region

The signal region is designed to provide the optimal separation between background and signal by imposing cuts on the kinematics of the final state particles. The choice of signal region was greatly inspired by the one used in the latest published ATLAS search [30] defined in table 8.1.

Signal region used in ATLAS search	
m_{ee} [GeV]	> 400
$m_{\mu\mu}$ [GeV]	> 400
Number of jets	≥ 2
Number of b-jets	0
Jet p_T [GeV]	> 100
H_T [GeV]	> 400
m_{jj} [GeV]	> 110

Table 8.1: Signal region for same-sign leptons used in the recent search performed by the ATLAS collaboration.

The distributions of some of the variables in table 8.1 are shown in figures 8.1-8.4 for preselected events. The cuts are motivated by separation between signal and background in the distributions.

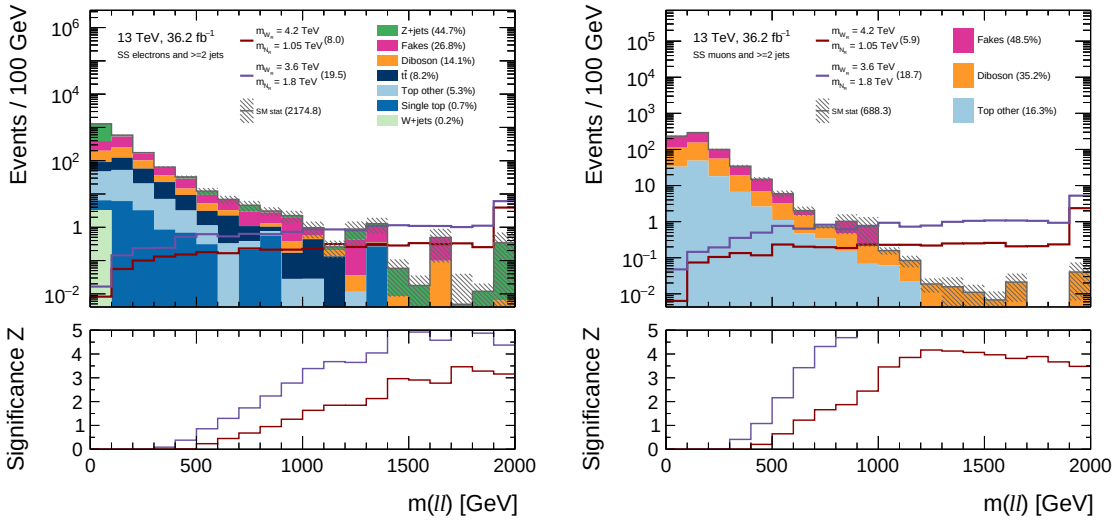

(a) $e^{\pm}e^{\pm}$ (b) $\mu^{\pm}\mu^{\pm}$

Figure 8.1: Distribution of the invariant mass of the two leptons. The last bin contains the overflow.

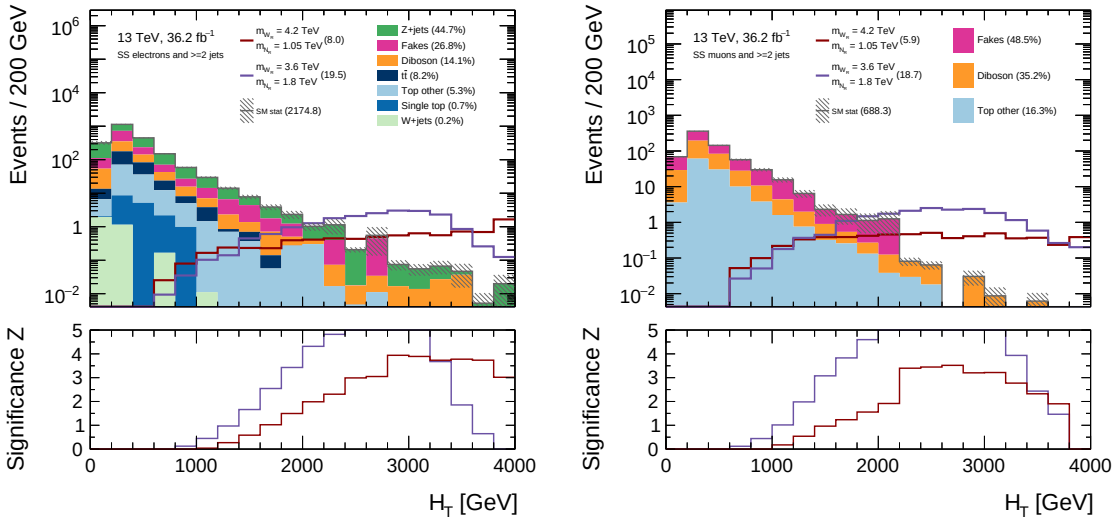

(a) $e^{\pm}e^{\pm}$ (b) $\mu^{\pm}\mu^{\pm}$

Figure 8.2: Distribution of the scalar p_T sum of the two leptons and the two leading jets. The last bin contains the overflow.

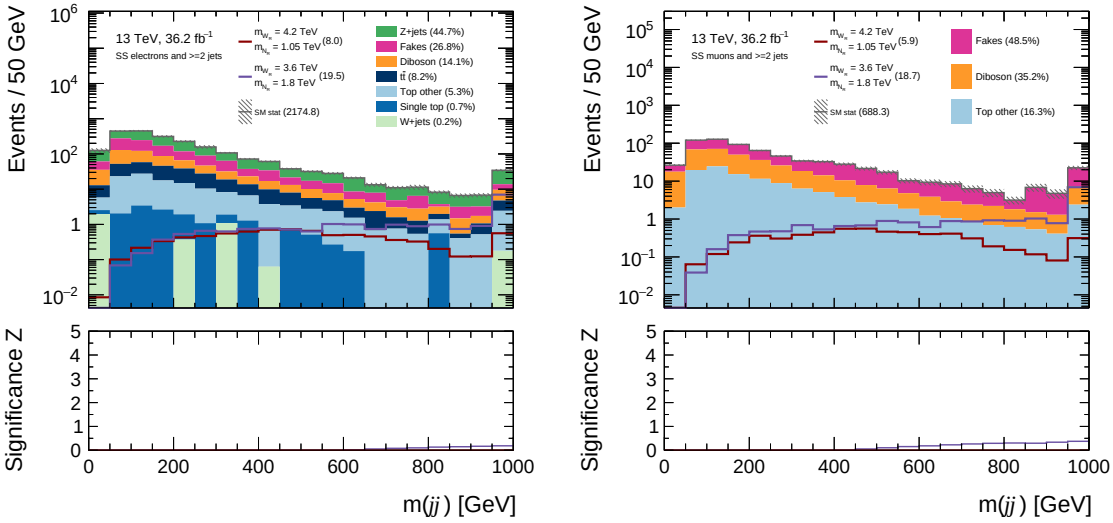

(a) $e^{\pm}e^{\pm}$ (b) $\mu^{\pm}\mu^{\pm}$

Figure 8.3: Distribution of the invariant mass of the two leading jets. The last bin contains the overflow.

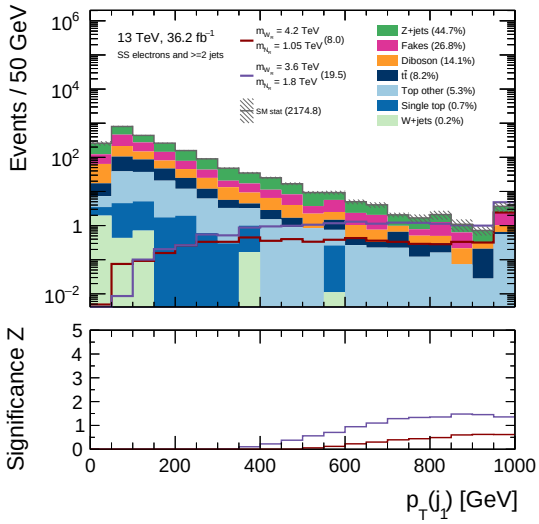

(a) $e^{\pm}e^{\pm}$

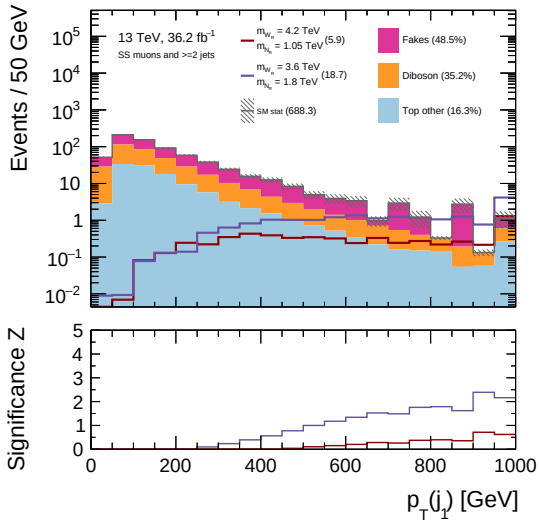

(b) $\mu^{\pm}\mu^{\pm}$

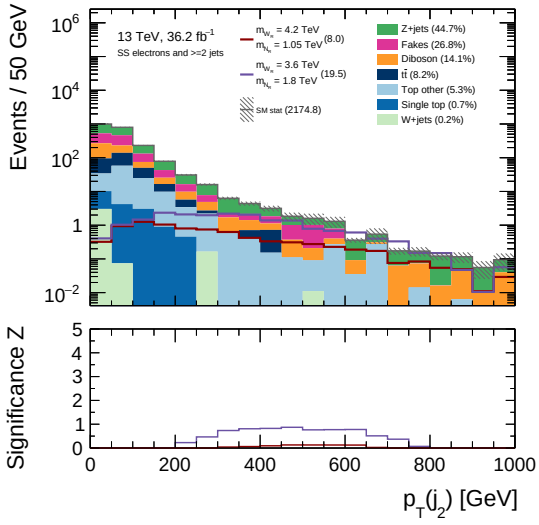

(c) $e^{\pm}e^{\pm}$

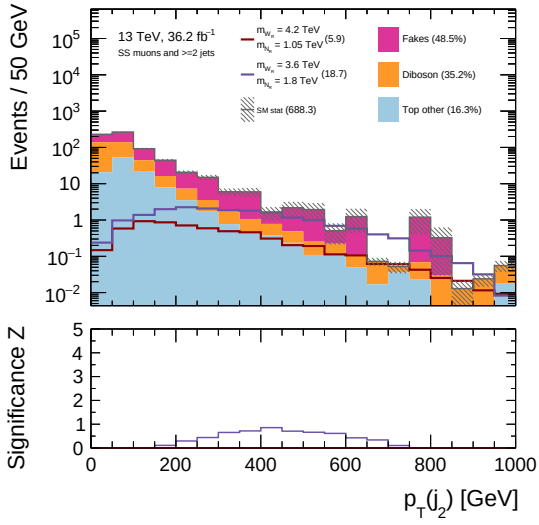

(d) $\mu^{\pm}\mu^{\pm}$

Figure 8.4: Distribution of the p_T of the leading (top) and the subleading (bottom) jet. The last bin contains the overflow.

The separation between background and signal at high m_{ll} in figure 8.1 clearly motivates a cut in this variable. The $m_{ll} > 400$ GeV cut used in the ATLAS search was found to be a good choice as it greatly decreases the expected background while hardly affecting the signal events. The cut on the invariant mass of the two leptons also vetoes the Z-peak, which removes much of the charge flip background from the $e^{\pm}e^{\pm}$ channel.

Figures 8.3 and 8.4 show the distributions of the dijet invariant mass m_{jj} and the transverse momentum p_T of the leading and subleading jets. As evident from the figures there is no clear difference in the distribution of background and signal events for these variables. The chosen cuts on the jet p_T and dijet invariant mass in this analysis are identical to the ones in table 8.1. A requirement of $m_{jj} > 110$ GeV suppresses jets from Z and W bosons decaying hadronically. An additional selection of $p_T > 100$ GeV is made for both jets to exploit the high energy of the KS process. The cuts made so far are summarized in table 8.2, and the resulting distributions of m_{lljj} and H_T are shown in figs. 8.5 and 8.6.

Preliminary signal region	
m_{ee} [GeV]	> 400
$m_{\mu\mu}$ [GeV]	> 400
Number of jets	≥ 2
Jet p_T [GeV]	> 100
m_{jj} [GeV]	> 110

Table 8.2: Preliminary signal region for same-sign leptons.

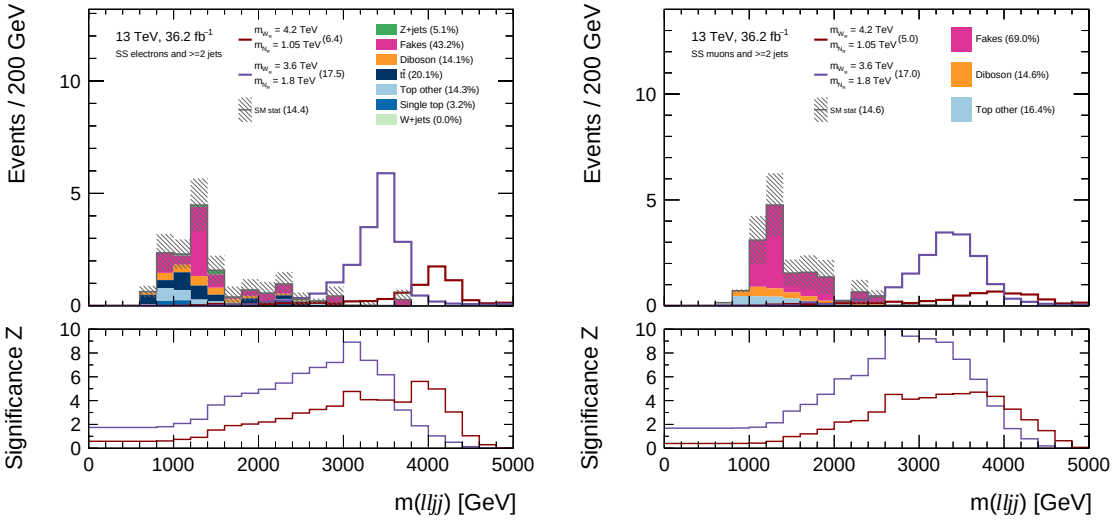

(a) $e^{\pm}e^{\pm}$ (b) $\mu^{\pm}\mu^{\pm}$

Figure 8.5: Distribution of the invariant mass of the two leptons and two leading jets, m_{lljj}, after imposing the cuts defined in table 8.2. The last bin contains the overflow.

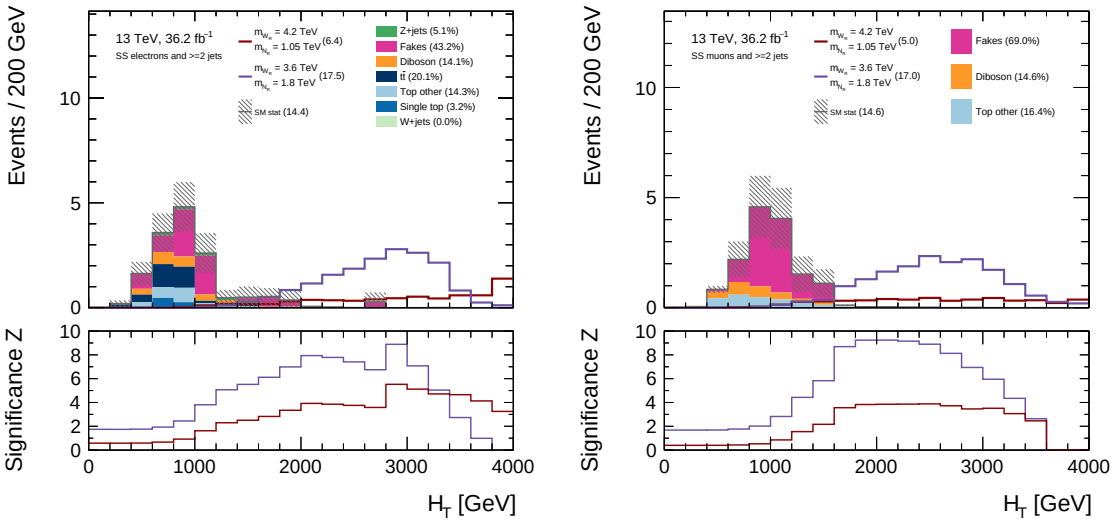

(a) $e^{\pm}e^{\pm}$ (b) $\mu^{\pm}\mu^{\pm}$

Figure 8.6: Distribution of the scalar p_T sum of the two leptons and the two leading jets after imposing the cuts defined in table 8.2. The last bin contains the overflow.

8.2.1 Veto on b-jets

A veto on b-jets was applied in the ATLAS search to reduce background from processes with top quarks and suppress leptons from heavy flavor decays. It was assumed that the veto would not affect the signal [60]. The distributions of m_{lljj} and H_T after applying a b-jet veto are shown in figures 8.7 and 8.8.

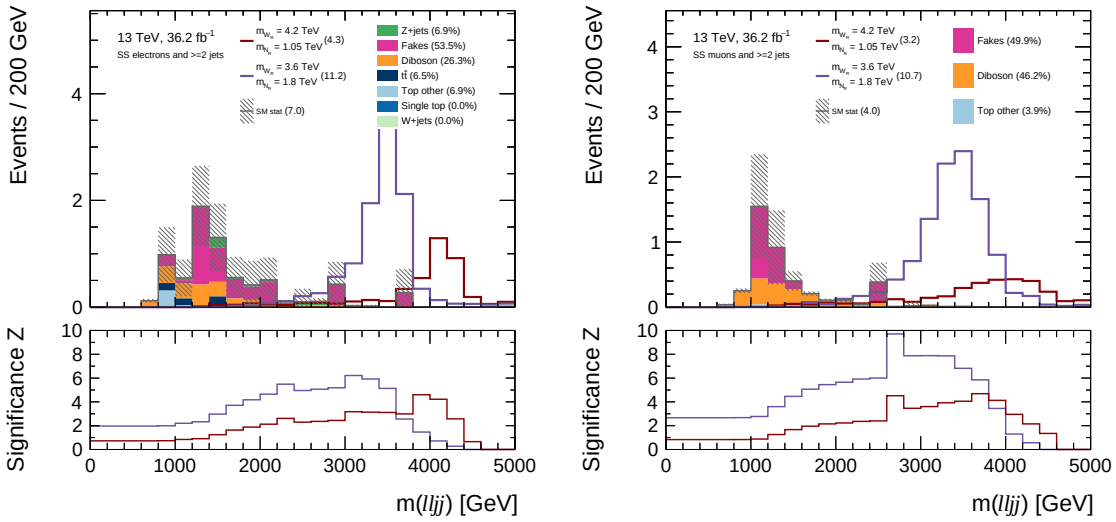

(a) $e^{\pm}e^{\pm}$ (b) $\mu^{\pm}\mu^{\pm}$

Figure 8.7: Distribution of the invariant mass of the two leptons and two leading jets, m_{lljj}, after imposing the cuts defined in table 8.2 and applying a b-jet veto. The last bin contains the overflow.

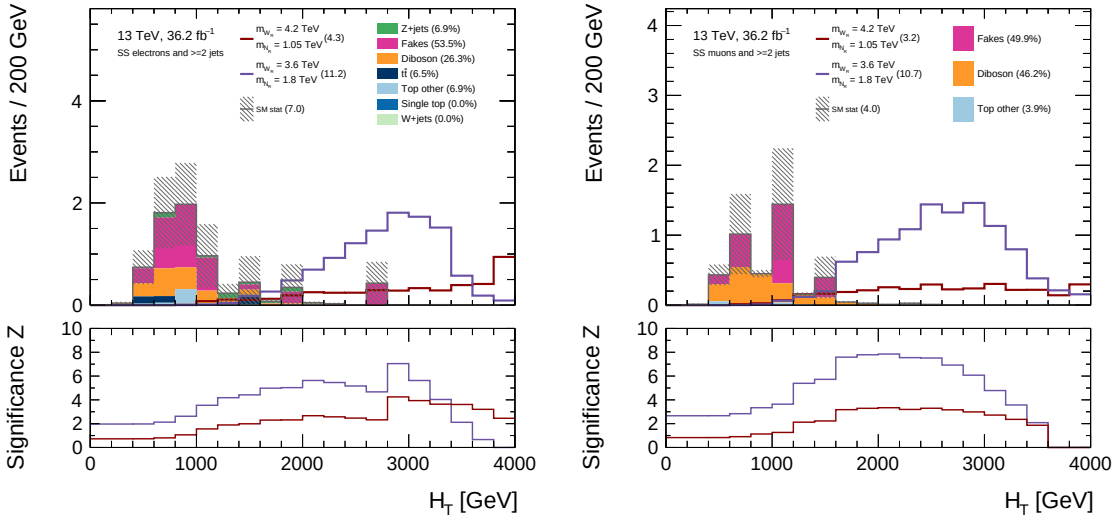

(a) $e^{\pm}e^{\pm}$ (b) $\mu^{\pm}\mu^{\pm}$

Figure 8.8: Distribution of the scalar p_T sum of the two leptons and the two leading jets after imposing the cuts defined in table 8.2 and applying a b-jet veto. The last bin contains the overflow.

As expected, the b-jet veto reduces background from all processes with top quarks and

from fakes. The veto does however decrease the expected significance, as several signal events do not pass the cut. The number of signal events in the electron and muon channel before and after applying the b-jet veto are shown in figures 8.9 and 8.10. As the sensitivity to the signal is worsened by vetoing b-jets, this cut is not applied in the SR in this thesis.

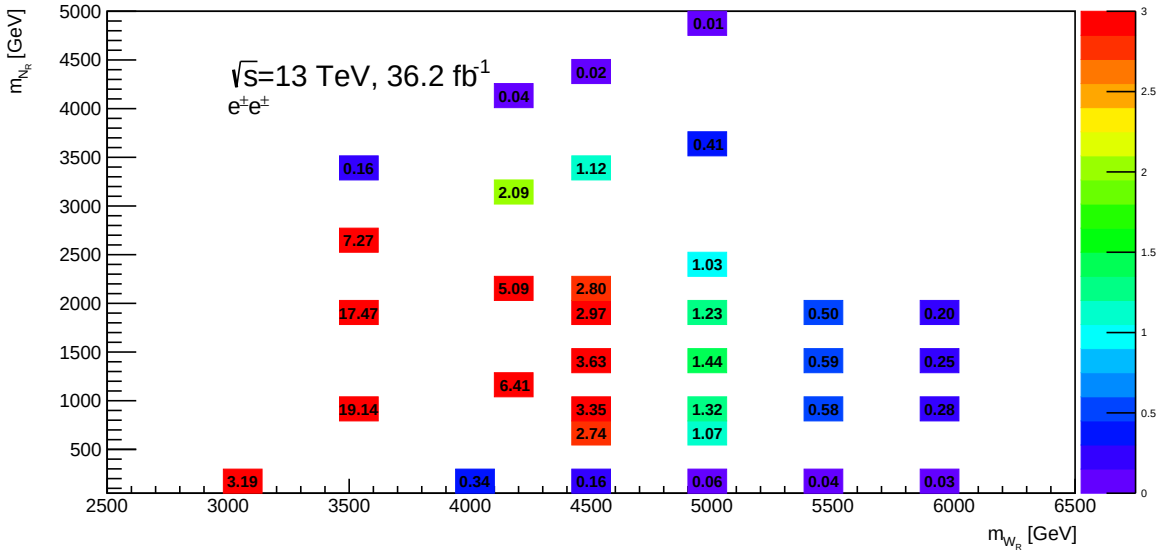

(a) $e^{\pm}e^{\pm}$, no veto on b-jets.

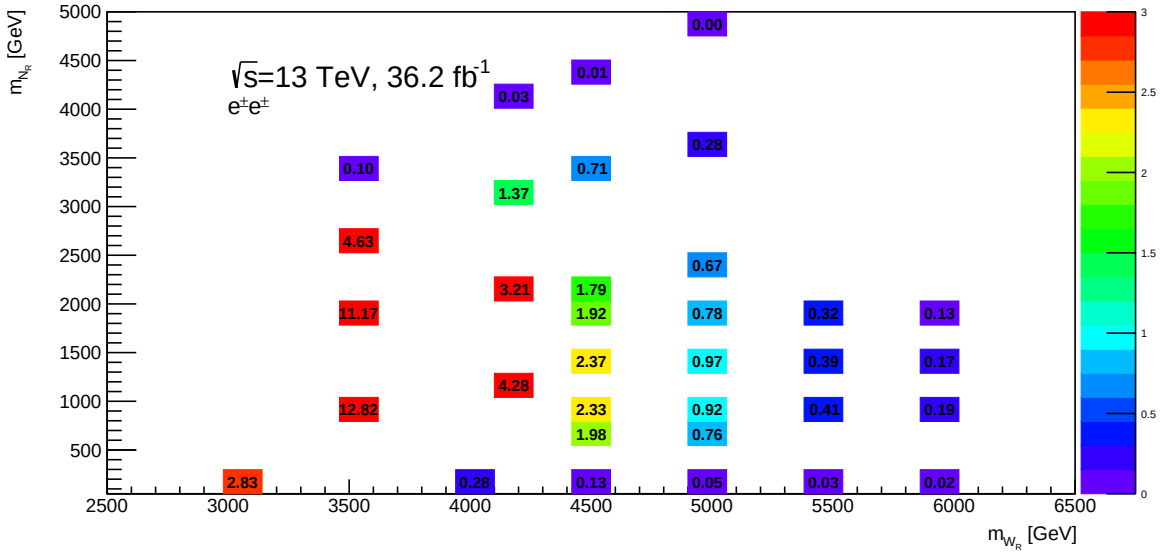

(b) $e^{\pm}e^{\pm}$, veto on b-jets.

Figure 8.9: Total number of signal events in the $m_{N_R} - m_{W_R}$ plane for the different signal samples in the preliminary signal region defined in table 8.2. The plots show the total number of signal events in the $e^{\pm}e^{\pm}$ before (a) and after applying (b) a veto on b-jets.

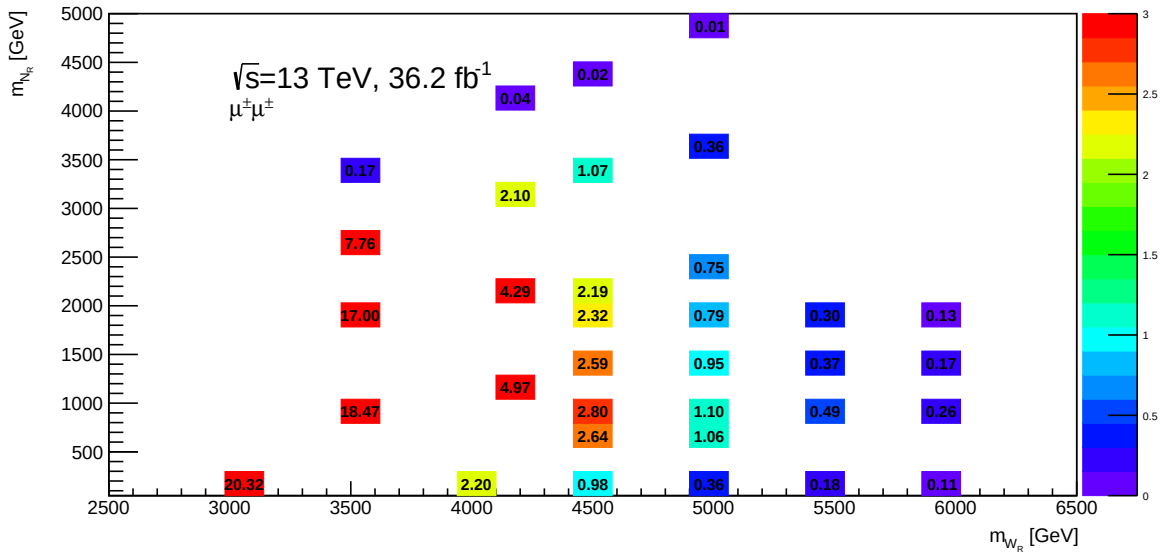

(a) $\mu^{\pm}\mu^{\pm}$, no veto on b-jets.

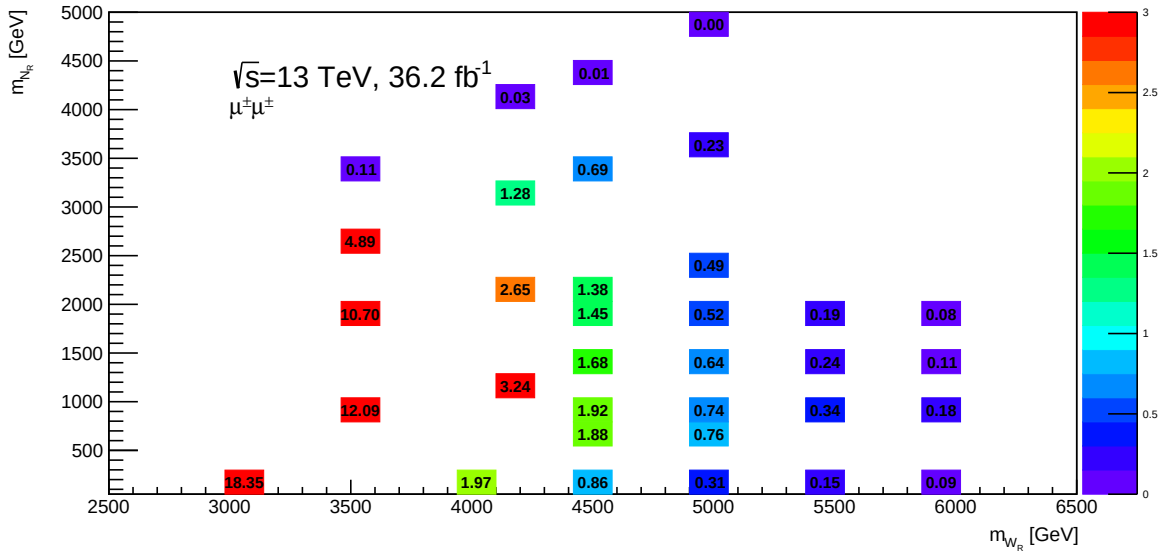

(b) $\mu^{\pm}\mu^{\pm}$, veto on b-jets.

Figure 8.10: Total number of signal events in the $m_{N_R} - m_{W_R}$ plane for the different signal samples in the preliminary signal region defined in table 8.2. The plots show the total number of signal events in the $\mu^{\pm}\mu^{\pm}$ before (a) and after applying (b) a veto on b-jets.

8.2.2 Sum of transverse momenta and total invariant mass

Due to some expected background at high m_{lljj}, the variable H_T was used as the discriminating variable in the ATLAS search [30]. This was found to be a good choice is this analysis too as the expected significance using this variable is higher than the one using m_{lljj} for lower W_R masses in the electron channel. The expected significance for the two variables are shown in figures 8.11 and 8.12.

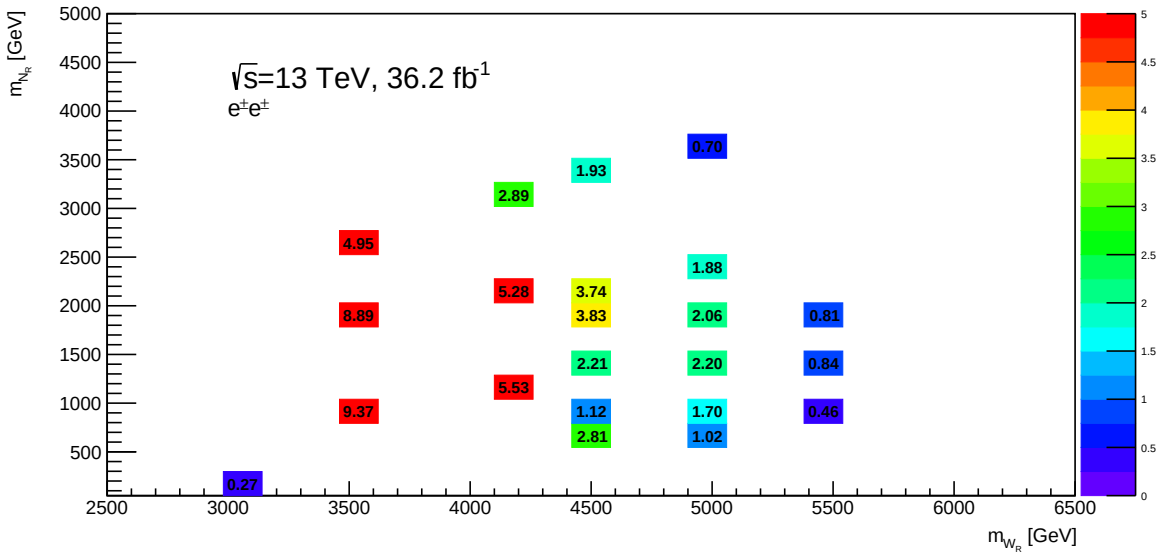

(a) H_T $(e^{\pm}e^{\pm})$

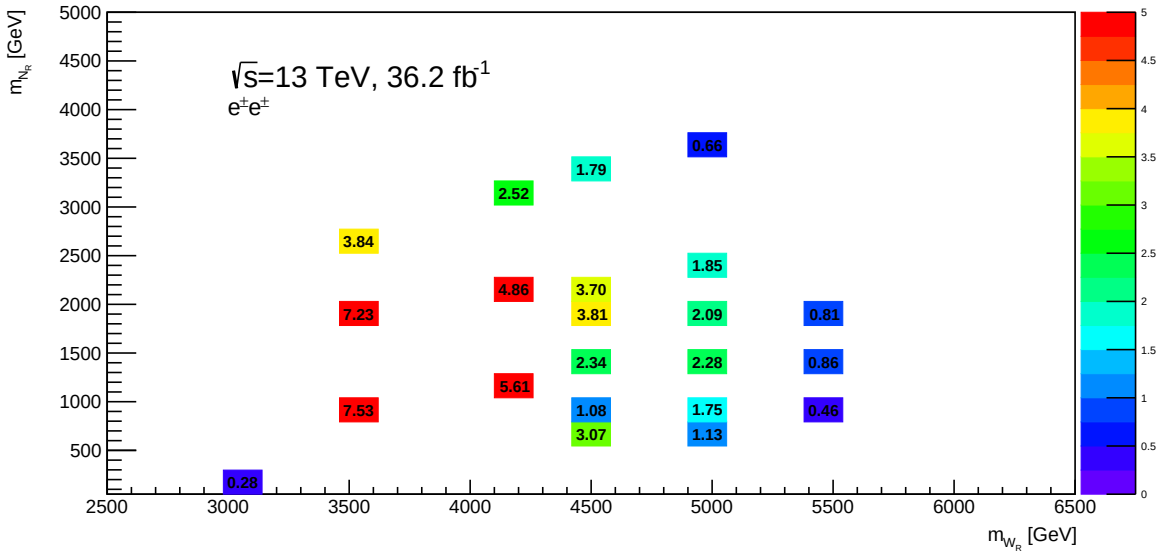

(b) m_{lljj} $(e^{\pm}e^{\pm})$

Figure 8.11: Expected significance in the $m_{N_R} - m_{W_R}$ plane in the preliminary signal region for the different signal samples using H_T (left) and m_{lljj} as the discriminating variable.

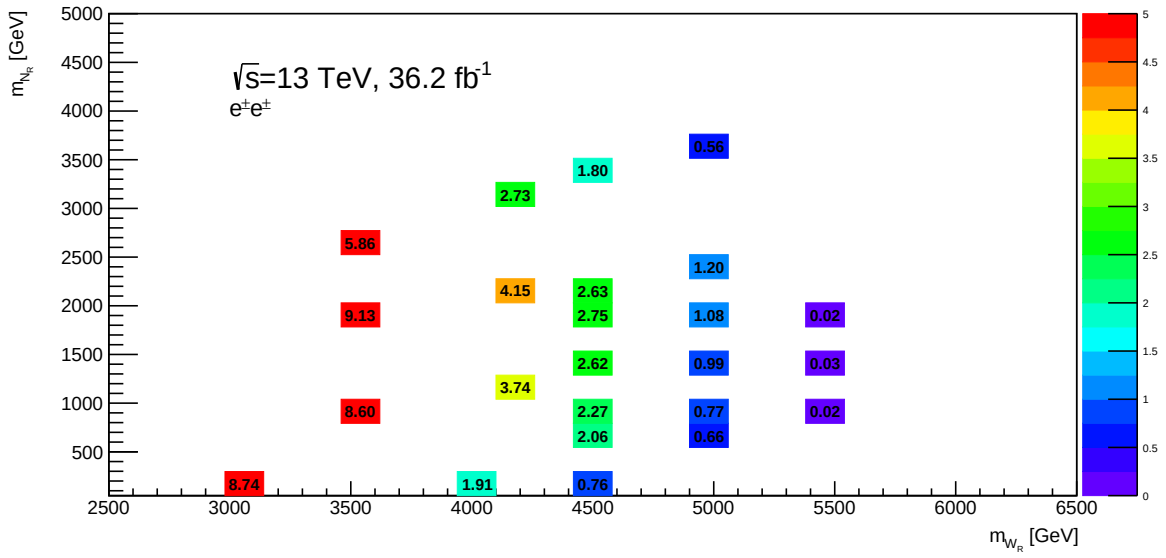

(a) H_T $(\mu^{\pm}\mu^{\pm})$

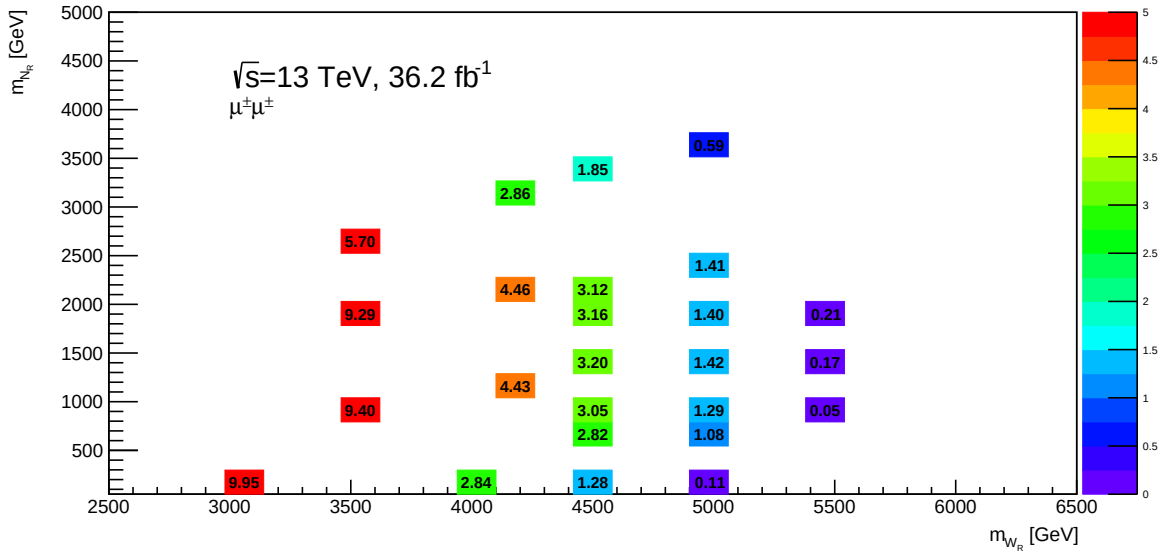

(b) m_{lljj} $(\mu^{\pm}\mu^{\pm})$

Figure 8.12: Expected significance in the $m_{N_R} - m_{W_R}$ plane in the preliminary signal region for the different signal samples using H_T (left) and m_{lljj} as the discriminating variable.

After the signal region has been chosen, the compatibility of the observed number of events with the $s + b$- and $b-$only hypotheses is evaluated by counting the number of events above the value of H_T that optimizes the expected significance. Hence the cut on H_T in the signal region is redundant. Instead a requirement of $m_{lljj} > 1000$ GeV was chosen to remove some background while maintaining sufficient statistics and a high number of signal events in the SR. The final signal region is summarized in the next subsection.

8.2.3 Final signal region

The final signal region is defined in table 8.3.

Signal region	
m_{ee} [GeV]	> 400
$m_{\mu\mu}$ [GeV]	> 400
Number of jets	≥ 2
Jet p_T [GeV]	> 100
m_{lljj} [GeV]	> 1000
m_{jj} [GeV]	> 110

Table 8.3: Signal region for same-sign leptons.

Chapter 9

Background estimation

Before looking for excesses in the data it must be verified that the background is modelled correctly. This is done by defining control and validation regions where no signal events are expected. The control regions (CRs) are used for background estimation, while validation regions (VRs) are used to verify that the estimation from the CRs still provides good agreement between data and background in a region orthogonal to the CR and the SR. If the agreement in the VR is deemed sufficient, the background is assumed to be well modelled in the signal region (SR), which is orthogonal to both the CR and the VR.

9.1 Prompt background

The prompt background mainly originates from processes with three or four charged leptons in the final state where only the same sign leptons are reconstructed. The main contribution to the prompt background comes from diboson and top processes.

To control the prompt background a control region with three or four charged signal leptons and at least two jets with $p_T > 50$ GeV is defined. The prompt CR is made orthogonal to the VR and SR by requiring $m_{ll} < 200$ GeV.

Distributions in the prompt CR are shown in figure 9.1. The lower plot shows the ratio between data and background. The hatched bands illustrate the statistical uncertainty in the MC, while the vertical bars on the data points indicate the statistical uncertainty in the data. The prompt background is found to be in reasonably good agreement with the data.

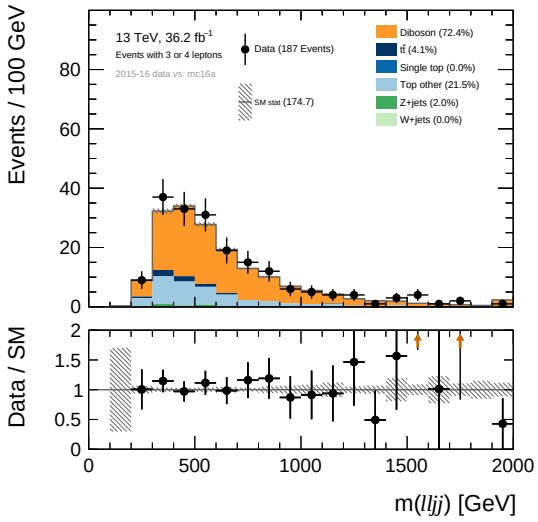

(a) Invariant mass of the two leading leptons and two leading jets.

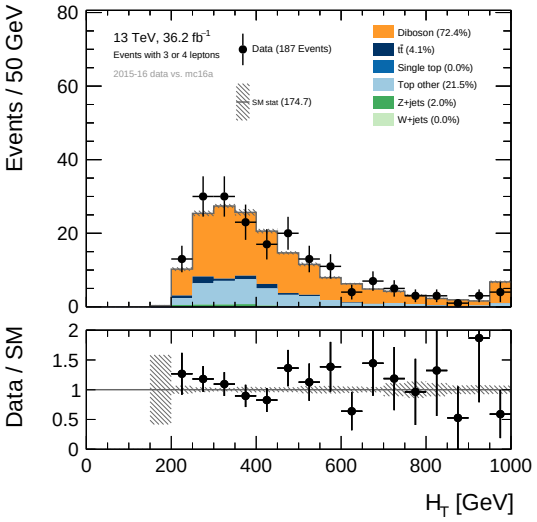

(b) Sum of transverse momenta of the two leading leptons and two leading jets.

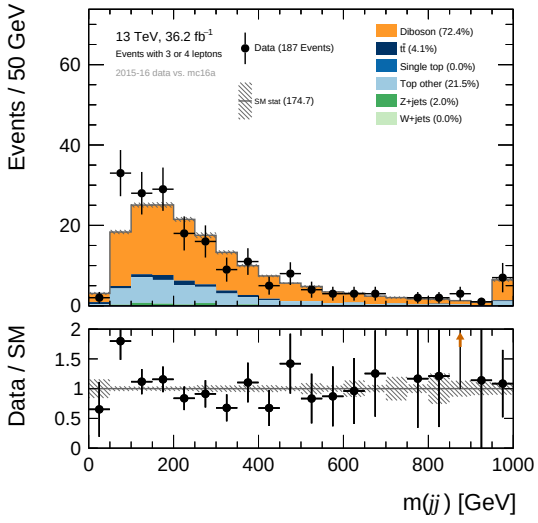

(c) Invariant mass of the two leading jets.

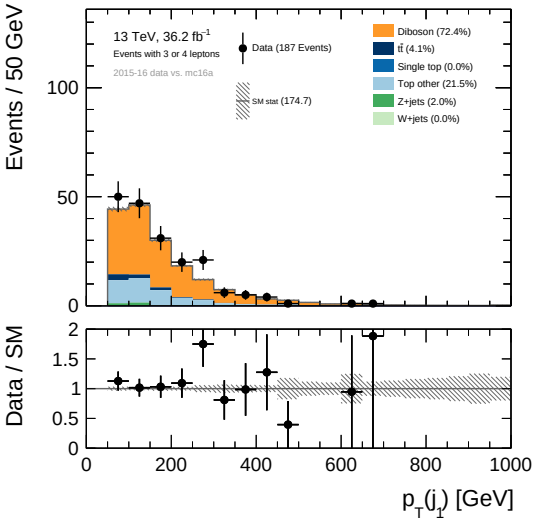

(d) Transverse momentum of the leading jet.

Figure 9.1: Distribution of (a) the invariant mass of the two leading leptons and two leading jets, (b) the sum of transverse momenta of the two leading leptons and two leading jets, (c) the invariant mass of the two leading jets and (d) the transverse momentum of the leading jet in events with three of four charged leptons and at least two jets.

9.2 Charge flip

An important source of background in the $e^{\pm}e^{\pm}$ channel comes from processes with oppositely charged electrons where one of the electrons is reconstructed with the wrong charge. Such background is commonly referred to as charge flip. All processes with a final state of opposite sign dileptons contribute to the charge flip background, with the main contribution coming from Z+jets and $t\bar{t}$ processes.

The electric charge of an electron is determined by the direction of its track curvature in

the inner detector. Charge misidentification occurs if the curvature is mismeasured or if the electron is associated with the wrong track. The electron can be reconstructed with the correct track but wrong charge if the electron has high transverse momentum p_T and hence a straight track in the ID. The combination of small curvature and few detector hits leads to low accuracy in the charge measurement.

Another source of charge misidentification is hard bremsstrahlung processes in the ID. When traversing the ID an electron can radiate a photon when in the presence of an atomic nucleus. If the photon undergoes pair production, $\gamma \rightarrow e^+e^-$, three tracks are present. This is known as a trident event. Of the three resulting tracks, two have the correct charge. If the bremsstrahlung process is hard, leading to an asymmetric distribution of the particle momenta, the track of the electron with the opposite charge of the primary electron can be reconstructed. Then the charge of the track is correctly measured, but as the reconstructed track is not associated with the correct electron the charge is misidentified. An example of a bremsstrahlung process leading to charge misidentification is illustrated in figure 9.2.

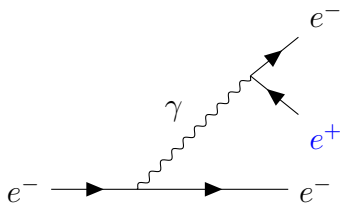

Figure 9.2: A bremsstrahlung process. The electron is reconstructed with the wrong charge if only the track corresponding to the blue lepton is reconstructed.

As Z bosons are produced frequently in collisions at the LHC, the Z+jets background constitutes the largest contribution to the charge flip background. The charge flip background can be studied by looking at a dilepton invariant mass region around the Z boson mass. As opposite sign dileptons are produced in the decay of Z bosons, a Z-peak in the same sign channel indicates that one of the electrons has had its charge misidentified.

A control region for SS Z+jets is defined by requiring exactly two signal electrons with an invariant mass close to the mass of the Z boson, 70 GeV $< m_{ll} <$ 110 GeV, and at least two jets with $p_T > 50$ GeV. In addition b-jets are vetoed to reduce contamination from $t\bar{t}$ processes. The distribution of the dilepton invariant mass, m_{ll}, in the SS Zjets CR is shown in figure 9.3.

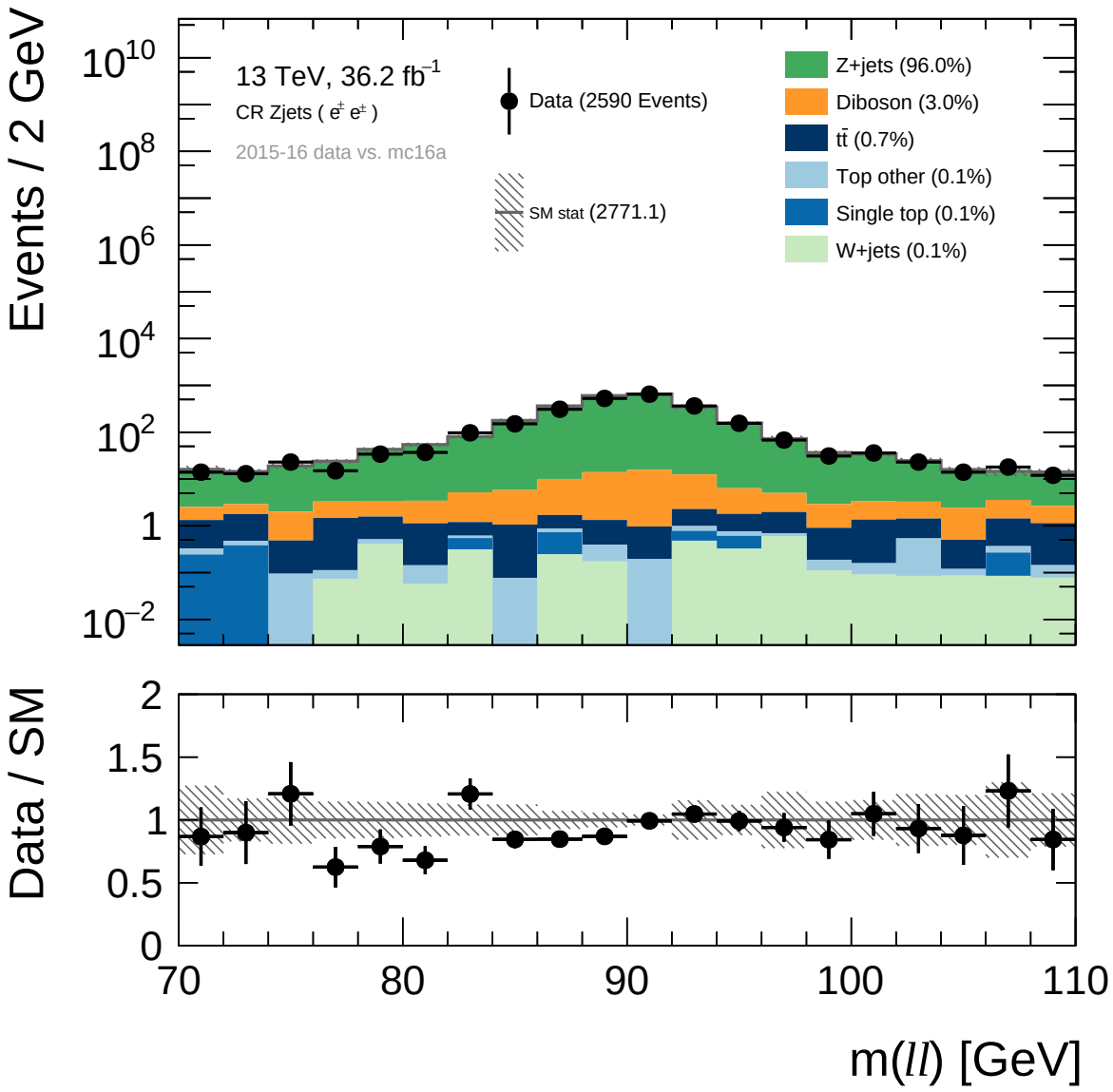

Figure 9.3: The distribution of the invariant mass of the two same sign leptons around the Z peak.

The control region has a high purity of Z+jets, and the peak around 91 GeV clearly shows the presence of a charge flipped electron. The data and background are found to be in good agreement.

The charge flip contribution is reduced using the Electron Charge ID Selector Tool (ECIDS) [55]. A boosted decision tree (BDT) is used to target charge misidentification due to bremsstrahlung and photon conversion [61]. For MediumLH electrons, which are used in this analysis, the ECIDS tool provides a benchmark signal efficiency of 97.46% and a rejection factor of 7.74 [55]. The yields in the Z+jets control region before and after applying the tool are given in table 9.1. As evident from the table, the tool greatly reduces the amount of charge flip background. The Z+jets contribution is reduced by a factor ~ 7, which is of the order of the benchmark rejection. The reduction factor in the data is ~ 6.

	Before ECIDS tool	After ECIDS tool
Data	2590	448
Total background	2774 ± 61	440 ± 21
Z+jets	2661 ± 60	388 ± 21
Diboson	86.6 ± 1.8	35.8 ± 1.0
$t\bar{t}$	19.0 ± 1.6	10.8 ± 1.2
Other	7.8 ± 2.0	4.7 ± 0.9

Table 9.1: Yields in the Z+jets control region before and after applying the ECIDS tool to reduce the charge flip background.

The electric charge of the muons is also measured in the MS, providing a longer lever arm and higher precision in the charge measurement. In addition the higher mass of the muons make them less likely to radiate photons in bremsstrahlung processes, so the charge flip background is negligible in the $\mu^{\pm}\mu^{\pm}$ channel.

9.3 Fakes

Fakes are generally not well modelled in the MC. The contribution from fakes was estimated using the data-driven matrix method, which is not discussed here. The interested reader is referred to ref. [62], whose author provided the fakes estimation for this thesis.

9.4 Validation

The validation region is used to validate the fakes estimation and charge flip reduction. The VR is defined in table 9.2

Validation region	
m_{ee} [GeV]	[200,400]
$m_{\mu\mu}$ [GeV]	[200,400]
Number of jets	≥ 2
Jet p_T [GeV]	> 50

Table 9.2: Validation region for same-sign leptons.

The distributions in the VR are shown in figures 9.4-9.6. The data and background are found to be in good agreement.

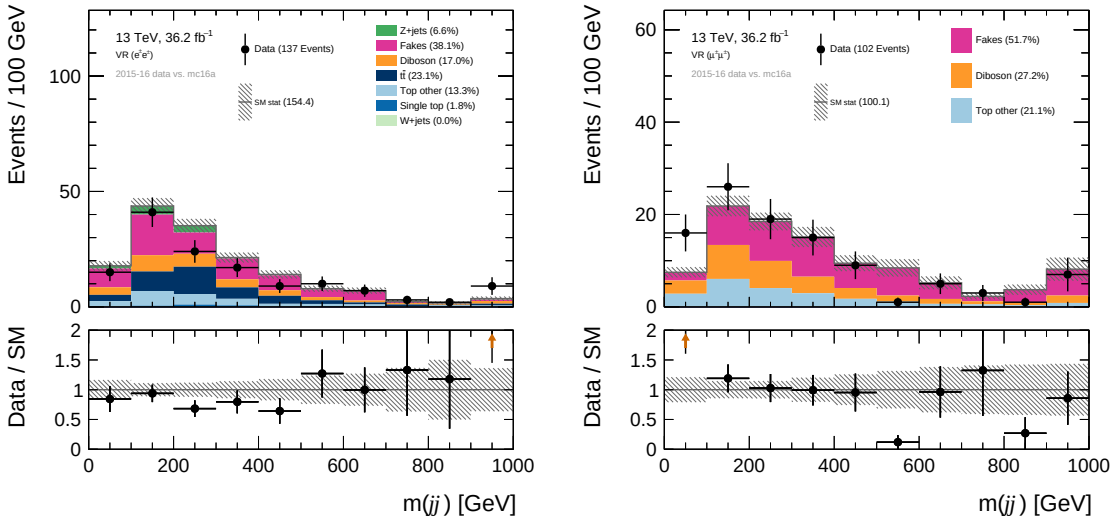

(a) VR ($e^{\pm}e^{\pm}$) (b) VR ($\mu^{\pm}\mu^{\pm}$)

Figure 9.4: Distribution of the invariant mass of the two leading jets, m_{jj}, in the validation region. The last bin contains the overflow.

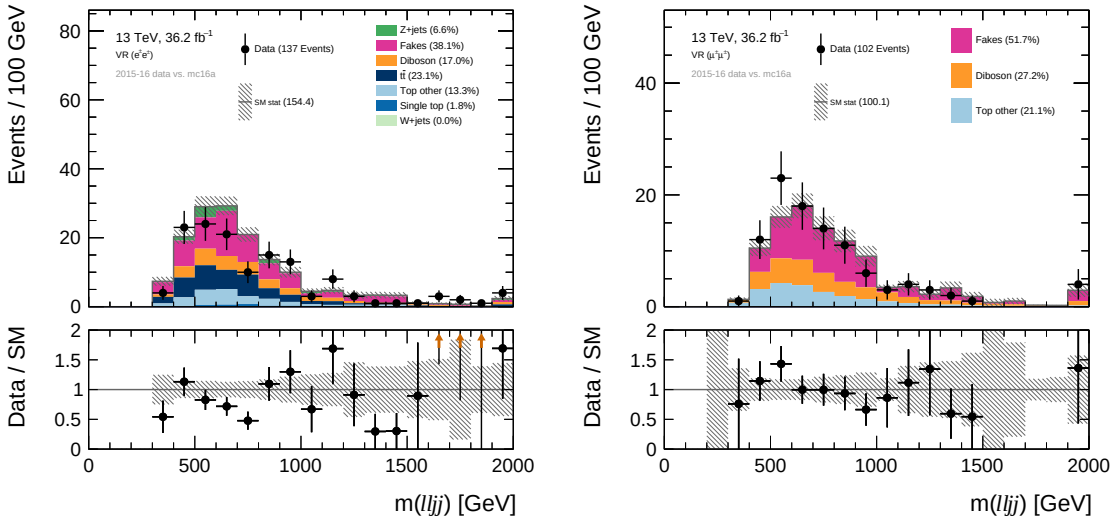

(a) VR ($e^{\pm}e^{\pm}$) (b) VR ($\mu^{\pm}\mu^{\pm}$)

Figure 9.5: Distribution of the invariant mass of the two leading leptons and the two leading jets, m_{lljj}, in the validation region. The last bin contains the overflow.

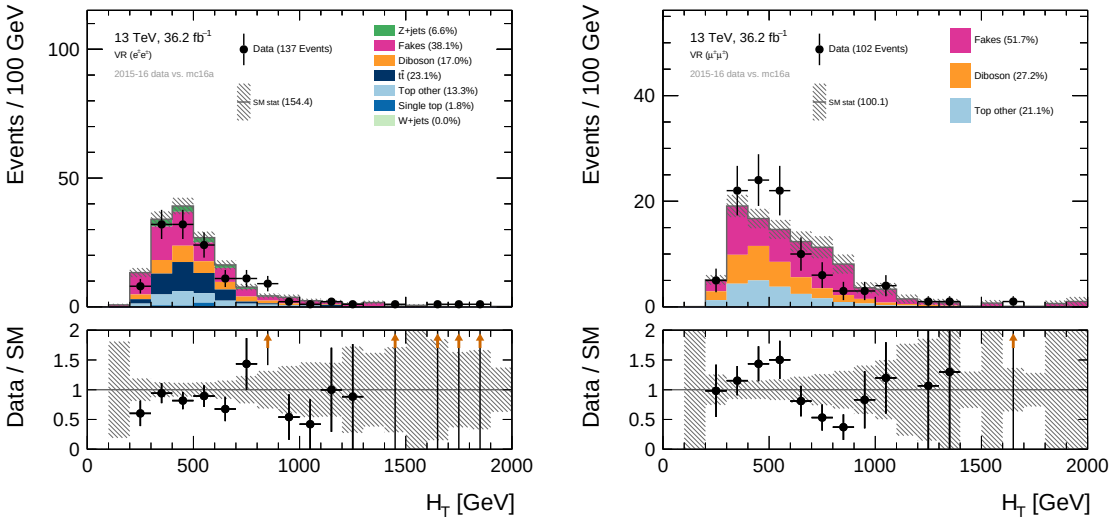

(a) VR ($e^{\pm}e^{\pm}$) (b) VR ($\mu^{\pm}\mu^{\pm}$)

Figure 9.6: Distribution of the scalar p_T sum of the two leading leptons and the two leading jets, H_T, in the validation region. The last bin contains the overflow.

Chapter 10

Results

The distributions of m_{lljj} and H_T in the SR are shown in figures 10.1 and 10.2 . No significant excess above the SM predictions is observed.

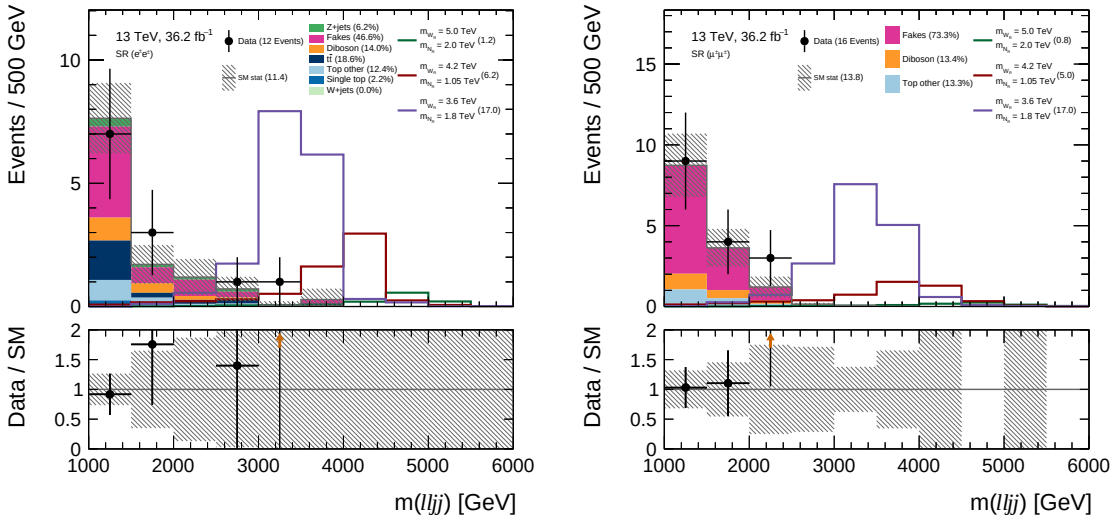

(a) SR ($e^{\pm}e^{\pm}$)

(b) SR ($\mu^{\pm}\mu^{\pm}$)

Figure 10.1: Distribution of the invariant mass of the two leptons and two leading jets, m_{lljj}, in the signal region. The last bin contains the overflow.

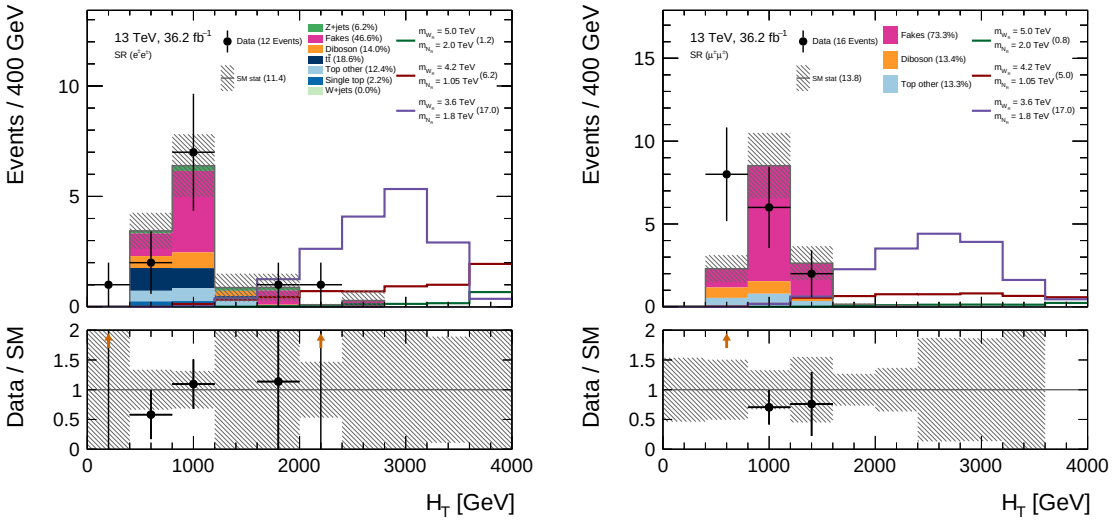

(a) SR ($e^{\pm}e^{\pm}$) (b) SR ($\mu^{\pm}\mu^{\pm}$)

Figure 10.2: Distribution of the scalar p_T sum of the two leptons and two leading jets, H_T, in the signal region. The last bin contains the overflow.

The lacking excess in the SR is used to put lower limits on the masses of the W_R boson and Majorana neutrino. This was done by counting the number observed and expected events above the value of H_T where the expected significance is at a maximum. The method fails for high W_R masses and for samples where the mass of the N_R is very close to the mass of the W_R as the cross sections for these samples are so small that close to zero signal events are expected. For these samples the expected significance never exceeds zero.

For the remaining samples zero events where observed above the H_T threshold that provides the highest expected significance. As mentioned in section 8.1 a signal can be excluded at 95% CL in the case of no observed events if the number of signal events is greater than three. The number of signal events in the SR region above the H_T are shown in figure 10.3. No events where observed for any of the points included in the plot.

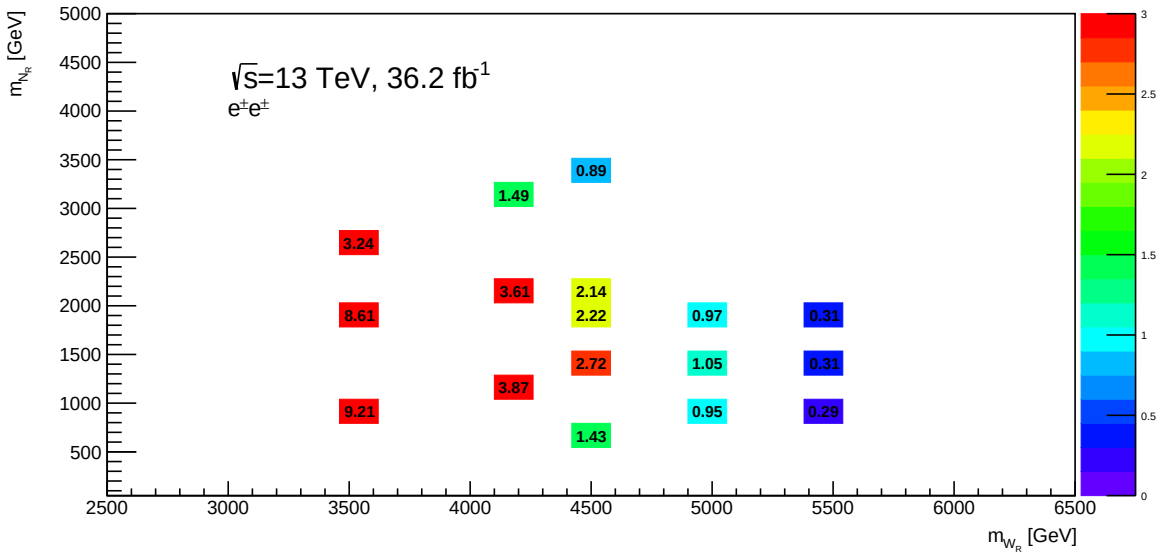

(a) Electron channel

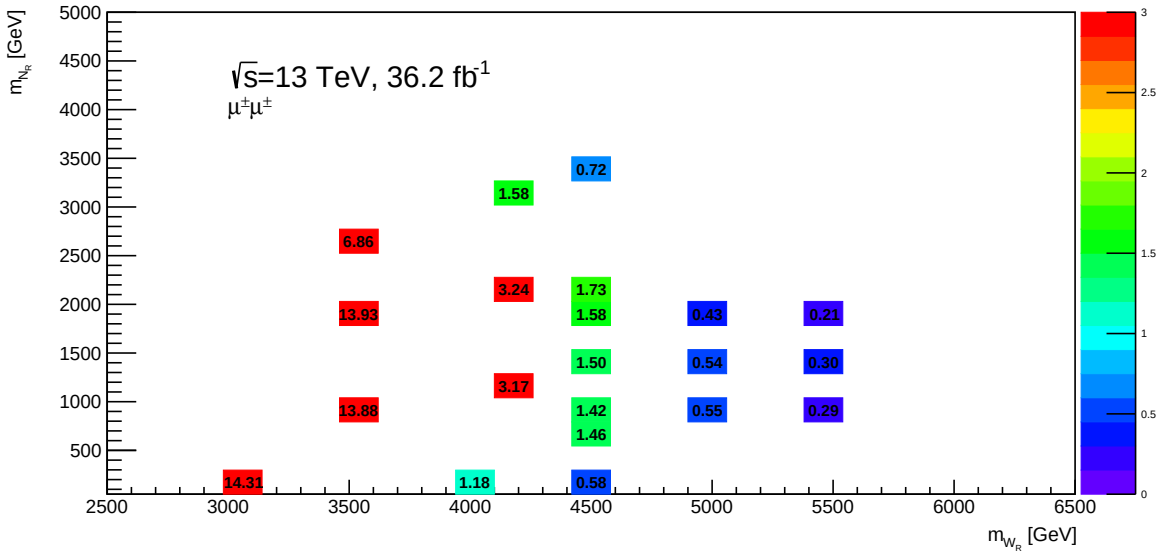

(b) Muon channel

Figure 10.3: Number of expected signal events in the SR above the threshold in H_T that maximises the expected significance. For all shown samples no date events where observed in the region, making all samples with more than three expected events excludable at 95% CL.

Based on the number of signal events in figure 10.3, the samples that can be excluded at 95% CL are shown in table 10.1 and 10.2.

The 95% CL exclusion plot from the most recent ATLAS search [30], which has provided the most stringent exclusions on the W_R boson and Majorana neutirno mass to date, is shown in figure 10.4. The plot includes results from the same sign (SS) and opposite sign (OS) search, as well as the combined results. Comparing with the results from the SS search, the exclusion limits obtained in this thesis are found to be consistent with the official results obtained by ATLAS.

Electron channel	
m_{W_R} [GeV]	m_{N_R} [GeV]
3600	900, 1800, 2700
4200	1050, 2100

Table 10.1: Samples that can be excluded at 95% CL in the electron channel.

Muon channel	
m_{W_R} [GeV]	m_{N_R} [GeV]
3000	100
3600	900, 1800, 2700
4200	1050, 2100

Table 10.2: Samples that can be excluded at 95% CL in the muon channel.

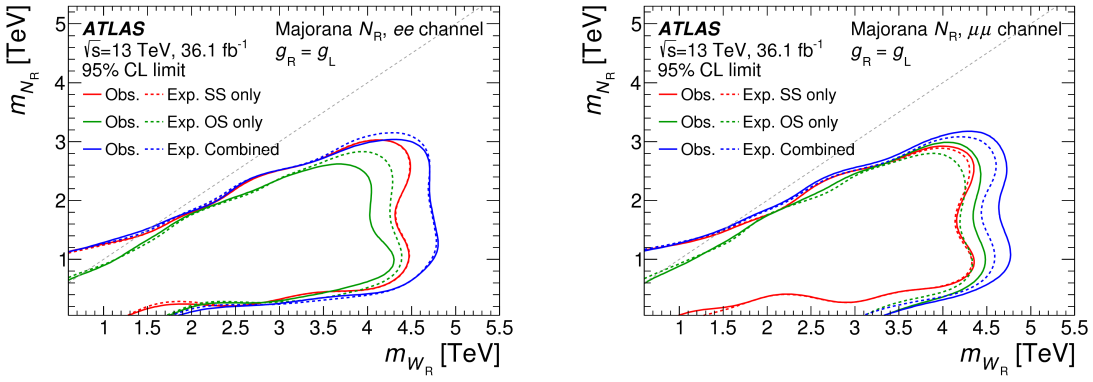

(a) Electron channel

(b) Muon channel

Figure 10.4: Observed and expected 95% CL exclusion contours from the recent ATLAS publication [30]. The plot includes results from both the same sign and opposite sign channels.

Conclusion

A search for right-handed heavy Majorana neutrinos and right-handed $W_R^{\pm}$ bosons was presented. Data from $\sqrt{s} = 13$ TeV proton-proton collisions collected by the ATLAS detector in 2015 and 2016 was used. The data correspond to an integrated luminosity of 36.2 fb^{-1}.

The final state considered consists of two same flavor leptons and two jets. Due to the Majorana nature of the heavy neutrino, there is a 50% probability of same sign leptons in the final state. Only the same sign channel was studied, as the expected number of background events is very small in this channel.

No significant excess was observed in the data, and the results were used to exclude points in the signal grid. The excluded W_R masses extend to 4.2 TeV for N_R masses up to 2.1 TeV, while the highest excluded N_R mass is 2.7 TeV for $m_{W_R} = 3.6$ TeV.

The same sign channel provides great separation between background and signal, and thus a high sensitivity to the LRSM signal. Due to small cross sections, higher mass points could not be excluded as the expected number was not sufficient for exclusion. This clearly motivates a new search using the full Run 2 data, as a higher luminosity increases the number of expected events. The 2017 and 2018 data had not yet been unblinded when this search was performed, so only results using the 2015 and 2016 data are included in this thesis. Control and validation regions were however studied including the 2017 data, and the background and data were found to be in good agreement. Unblinding the data for the rest of Run 2 would certainly be interesting, as the potential for discovery or exclusion is high in the same sign channel.

Bibliography

[1] Y. Fukuda et al. "Evidence for Oscillation of Atmospheric Neutrinos." In: *Phys. Rev. Lett.* 81 (8 1998), pp. 1562–1567. DOI: 10.1103/PhysRevLett.81.1562.

[2] Q. R. Ahmad et al. "Direct Evidence for Neutrino Flavor Transformation from Neutral-Current Interactions in the Sudbury Neutrino Observatory." In: *Phys. Rev. Lett.* 89 (1 2002), p. 011301. DOI: 10.1103/PhysRevLett.89.011301.

[3] M. Tanabashi et al. "Review of Particle Physics." In: *Phys. Rev. D* 98 (3 2018), p. 030001. DOI: 10.1103/PhysRevD.98.030001.

[4] Sheldon L. Glashow. "Partial-symmetries of weak interactions." In: *Nuclear Physics* 22.4 (1961), pp. 579–588. ISSN: 0029-5582. DOI: 10.1016/0029-5582(61)90469-2.

[5] Steven Weinberg. "A Model of Leptons." In: *Phys. Rev. Lett.* 19 (21 1967), pp. 1264–1266. DOI: 10.1103/PhysRevLett.19.1264.

[6] Abdus Salam. "Weak and Electromagnetic Interactions." In: *Conf. Proc.* C680519 (1968), pp. 367–377.

[7] S. L. Glashow, J. Iliopoulos, and L. Maiani. "Weak Interactions with Lepton-Hadron Symmetry." In: *Phys. Rev. D* 2 (7 1970), pp. 1285–1292. DOI: 10.1103/PhysRevD.2.1285.

[8] Peter W. Higgs. "Spontaneous Symmetry Breakdown without Massless Bosons." In: *Phys. Rev.* 145 (4 1966), pp. 1156–1163. DOI: 10.1103/PhysRev.145.1156.

[9] F. Englert and R. Brout. "Broken Symmetry and the Mass of Gauge Vector Mesons." In: *Phys. Rev. Lett.* 13 (9 1964), pp. 321–323. DOI: 10.1103/PhysRevLett.13.321.

[10] Georges Aad et al. "Observation of a new particle in the search for the Standard Model Higgs boson with the ATLAS detector at the LHC." In: *Phys. Lett.* B716 (2012), pp. 1–29. DOI: 10.1016/j.physletb.2012.08.020. arXiv: 1207.7214 [hep-ex].

[11] Serguei Chatrchyan et al. "Observation of a new boson at a mass of 125 GeV with the CMS experiment at the LHC." In: *Phys. Lett.* B716 (2012), pp. 30–61. DOI: 10.1016/j.physletb.2012.08.021. arXiv: 1207.7235 [hep-ex].

[12] Universität Zürich. *Standard Model*. https://www.physik.uzh.ch/groups/serra/StandardModel.html. Accessed: 08.04.2019.

[13] Michael E. Peskin and Daniel V. Schroeder. *An Introduction to Quantum Field Theory*. Westview Press, 2016.

[14] Antonio Pich. "Aspects of quantum chromodynamics." In: *Proceedings, Summer School in Particle Physics: Trieste, Italy, June 21-July 9, 1999*. 1999, pp. 53–102. arXiv: hep-ph/0001118 [hep-ph].

[15] Antonio Pich. "The Standard model of electroweak interactions." In: *The Standard model of electroweak interactions*. [,1(2007)]. 2008, pp. 1–49. arXiv: 0705.4264 [hep-ph].

[16] Chien-Yi Chen and P. S. Bhupal Dev. "Multilepton collider signatures of heavy Dirac and Majorana neutrinos." In: *Phys. Rev. D* 85 (9 2012), p. 093018. DOI: 10.1103/PhysRevD.85.093018.

[17] G. Senjanovic. "Neutrino mass: From LHC to grand unification." In: *Riv. Nuovo Cim.* 34 (2011), pp. 1–68. DOI: 10.1393/ncr/i2011-10061-8.

[18] Ettore Majorana. "Teoria simmetrica dell'elettrone e del positrone." In: *Il Nuovo Cimento (1924-1942)* 14.4 (2008), p. 171. ISSN: 1827-6121. DOI: 10.1007/BF02961314.

[19] Peter Minkowski. "$\mu \to e\gamma$ at a rate of one out of 10^9 muon decays?" In: *Physics Letters B* 67 (1977), pp. 421–428. DOI: 10.1016/0370-2693(77)90435-X.

[20] Jogesh C. Pati and Abdus Salam. "Lepton Number as the Fourth Color." In: *Phys. Rev.* D10 (1974). [Erratum: Phys. Rev.D11,703(1975)], pp. 275–289. DOI: 10.1103/PhysRevD.10.275.

[21] Rabindra N. Mohapatra and Jogesh C. Pati. "Left-right gauge symmetry and an "isoconjugate" model of CP violation." In: *Phys. Rev. D* 11 (3 1975), pp. 566–571. DOI: 10.1103/PhysRevD.11.566.

[22] R. N. Mohapatra and J. C. Pati. ""Natural" left-right symmetry." In: *Phys. Rev. D* 11 (9 1975), pp. 2558–2561. DOI: 10.1103/PhysRevD.11.2558.

[23] G. Senjanovic and R. N. Mohapatra. "Exact left-right symmetry and spontaneous violation of parity." In: *Phys. Rev. D* 12 (5 1975), pp. 1502–1505. DOI: 10.1103/PhysRevD.12.1502.

[24] Goran Senjanovic. "Is Left-Right Symmetry the Key?" In: *Mod. Phys. Lett.* A32.04 (2017), p. 1730004. DOI: 10.1142/S021773231730004X. arXiv: 1610.04209 [hep-ph].

[25] Yorikiyo Nagashima. *Beyond the Standard Model of Elementary Particle Physics*. Wiley-VCH, 2014.

[26] Rabindra N. Mohapatra and Goran Senjanovi . "Neutrino Mass and Spontaneous Parity Nonconservation." In: *Phys. Rev. Lett.* 44 (14 1980), pp. 912–915. DOI: 10.1103/PhysRevLett.44.912.

[27] Wai-Yee Keung and Goran Senjanovic. "Majorana Neutrinos and the Production of the Right-Handed Charged Gauge Boson." In: *Phys. Rev. Lett.* 50 (19 1983), pp. 1427–1430. DOI: 10.1103/PhysRevLett.50.1427.

[28] Morad Aaboud et al. "Search for a right-handed gauge boson decaying into a high-momentum heavy neutrino and a charged lepton in pp collisions with the ATLAS detector at $\sqrt{s} = 13$ TeV." In: (2019). arXiv: 1904.12679 [hep-ex].

[29] Stefano Bertolini, Alessio Maiezza, and Fabrizio Nesti. "Present and future K and B meson mixing constraints on TeV scale left-right symmetry." In: *Phys. Rev. D* 89 (9 2014), p. 095028. DOI: 10.1103/PhysRevD.89.095028.

[30] Morad Aaboud et al. "Search for heavy Majorana or Dirac neutrinos and right-handed W gauge bosons in final states with two charged leptons and two jets at $\sqrt{s} = 13$ TeV with the ATLAS detector." In: *JHEP* 01 (2019), p. 016. DOI: 10.1007/JHEP01(2019)016. arXiv: 1809.11105 [hep-ex].

[31] A. Einstein. "Ist die Trägheit eines Körpers von seinem Energieinhalt abhängig?" In: *Annalen der Physik* 323.13 (1905), pp. 639–641. DOI: 10.1002/andp.19053231314. eprint: https://onlinelibrary.wiley.com/doi/pdf/10.1002/andp.19053231314.

[32] Lyndon Evans and Philip Bryant. "LHC Machine." In: *Journal of Instrumentation* 3.08 (2008), S08001–S08001. DOI: 10.1088/1748-0221/3/08/s08001.

[33] A. D. Martin et al. "Parton distributions for the LHC." In: *Eur. Phys. J.* C63 (2009), pp. 189–285. DOI: 10.1140/epjc/s10052-009-1072-5. arXiv: 0901.0002 [hep-ph].

[34] Sylvie Braibant, Giorgio Giacomelli, and Maurizio Spurio. *Particles and Fundamental Interactions*. Springer, 2012.

[35] Shirley Weishi Li and John F. Beacom. "Spallation Backgrounds in Super-Kamiokande Are Made in Muon-Induced Showers." In: *Phys. Rev.* D91.10 (2015), p. 105005. DOI: 10.1103/PhysRevD.91.105005. arXiv: 1503.04823 [hep-ph].

[36] Mark Thompson. *Modern Particle Physics*. Cambridge University Press, 2013.

[37] The ATLAS Collaboration. *How ATLAS detects particles: diagram of particle paths in the detector*. http://cds.cern.ch/record/1505342?ln=en. Accessed: 20.04.2019.

[38] The ATLAS Collaboration. "The ATLAS Experiment at the CERN Large Hadron Collider." In: *Journal of Instrumentation* 3.08 (2008), S08003–S08003. DOI: 10.1088/1748-0221/3/08/s08003.

[39] The ATLAS Collaboration. *Computer generated image of the whole ATLAS detector*. http://cdsweb.cern.ch/record/1095924. Accessed: 18.04.2019.

[40] Morad Aaboud et al. "Performance of the ATLAS Trigger System in 2015." In: *Eur. Phys. J.* C77.5 (2017), p. 317. DOI: 10.1140/epjc/s10052-017-4852-3. arXiv: 1611.09661 [hep-ex].

[41] M. Aaboud et al. "Electron efficiency measurements with the ATLAS detector using 2012 LHC proton–proton collision data." In: *The European Physical Journal C* 77.3 (2017), p. 195. ISSN: 1434-6052. DOI: 10.1140/epjc/s10052-017-4756-2.

[42] Morad Aaboud et al. "Electron reconstruction and identification in the ATLAS experiment using the 2015 and 2016 LHC proton-proton collision data at $\sqrt{s} = 13$ TeV." In: *Submitted to: Eur. Phys. J.* (2019). arXiv: 1902.04655 [physics.ins-det].

[43] Atlas Collaboration et al. "Muon reconstruction performance of the ATLAS detector in proton–proton collision data at $\sqrt{s}$=13 TeV." In: *The European Physical Journal C* 76.5 (2016), p. 292. ISSN: 1434-6052. DOI: 10.1140/epjc/s10052-016-4120-y.

[44] Matteo Cacciari, Gavin P. Salam, and Gregory Soyez. "The anti-k_t jet clustering algorithm." In: *JHEP* 04 (2008), p. 063. DOI: 10.1088/1126-6708/2008/04/063. arXiv: 0802.1189 [hep-ph].

[45] A. Hrynevich. "ATLAS jet and missing energy reconstruction, calibration and performance in LHC Run-2." In: *JINST* 12.06 (2017), p. C06038. DOI: 10.1088/1748-0221/12/06/C06038.

[46] *Tagging and suppression of pileup jets with the ATLAS detector*. Tech. rep. ATLAS-CONF-2014-018. Geneva: CERN, 2014.

[47] The ATLAS collaboration et al. "Measurements of b-jet tagging efficiency with the ATLAS detector using ttŕ$$ t\overline{t}$$eventsats = 13$$\sqrt{s} = 13$$TeV." In: *Journal of High Energy Physics* 2018.8 (2018), p. 89. ISSN: 1029-8479. DOI: 10.1007/JHEP08(2018)089.

[48] The ATLAS Collaboration. *Lowest un-prescaled triggers per data-taking period*. https://twiki.cern.ch/twiki/bin/view/Atlas/LowestUnprescaled. Accessed: 13.05.2019.

[49] S. Agostinelli et al. "Geant4-a simulation toolkit." In: *Nuclear Instruments and Methods in Physics Research Section A: Accelerators, Spectrometers, Detectors and Associated Equipment* 506.3 (2003), pp. 250–303. ISSN: 0168-9002. DOI: 10.1016/S0168-9002(03)01368-8.

[50] T Gleisberg et al. "Event generation with SHERPA 1.1." In: *Journal of High Energy Physics* 2009.02 (2009), pp. 007–007. DOI: 10.1088/1126-6708/2009/02/007.

[51] Torbjörn Sjöstrand, Stephen Mrenna, and Peter Skands. "A brief introduction to PYTHIA 8.1." In: *Computer Physics Communications* 178.11 (2008), pp. 852–867. ISSN: 0010-4655. DOI: 10.1016/j.cpc.2008.01.036.

[52] Simone Alioli et al. "A general framework for implementing NLO calculations in shower Monte Carlo programs: the POWHEG BOX." In: *Journal of High Energy Physics* 2010.6 (2010), p. 43. ISSN: 1029-8479. DOI: 10.1007/JHEP06(2010)043.

[53] J. Alwall et al. "The automated computation of tree-level and next-to-leading order differential cross sections, and their matching to parton shower simulations." In: *Journal of High Energy Physics* 2014.7 (2014), p. 79. ISSN: 1029-8479. DOI: 10.1007/JHEP07(2014)079.

[54] The ATLAS Collaboration. *MCTruthClassifier*. https://twiki.cern.ch/twiki/bin/view/AtlasProtected/MCTruthClassifier. Accessed: 29.04.2019.

[55] The ATLAS Collaboration. *Electron Charge ID Selector Tool*. https://twiki.cern.ch/twiki/bin/viewauth/AtlasProtected/ElectronChargeFlipTaggerTool. Accessed: 01.05.2019.

[56] Olaf Benche et al. *Data Analysis in High Energy Physics*. Wiley-VCH, 2013.

[57] Robert D. Cousins, Kathryn E. Hymes, and Jordan Tucker. "Frequentist evaluation of intervals estimated for a binomial parameter and for the ratio of Poisson means." In: *Nuclear Instruments and Methods in Physics Research Section A: Accelerators, Spectrometers, Detectors and Associated Equipment* 612.2 (2010), pp. 388–398. ISSN: 0168-9002. DOI: https://doi.org/10.1016/j.nima.2009.10.156.

[58] A L Read. "Presentation of search results: theCLstechnique." In: *Journal of Physics G: Nuclear and Particle Physics* 28.10 (2002), pp. 2693–2704. DOI: 10.1088/0954-3899/28/10/313.

[59] Magnar Kopangen Bugge. "Search for new charged bosons and dark matter in final states with one lepton and missing transverse energy with the ATLAS detector at the LHC." PhD thesis. University of Oslo, 2015.

[60] Xanthe Hoad et al. *Search for heavy Majorana or Dirac neutrinos and right-handed W gauge bosons in final states with two charged leptons and two jets at $\sqrt{s}$=13 TeV with the ATLAS collaboration*. Tech. rep. ATL-COM-PHYS-2017-704. Geneva: CERN, 2017.

[61] The ATLAS Collaboration. *Electron Charge Flip Tagger Development*. https://indico.cern.ch/event/578089/contributions/2341456/attachments/1356262/2050030/20161017_egamma.pdf. Accessed: 01.05.2019.

[62] Eirik Gramstad. "Searches for Supersymmetry in Di-Lepton Final States with the ATLAS Detector at s = 7 TeV." PhD thesis. University of Oslo, 2013.